Leading Edge
Review

Cell

A Glimpse of Structural Biology through X-Ray Crystallography

Yigong Shi[1,*]
[1]Center for Structural Biology, Tsinghua-Peking Joint Center for Life Sciences, School of Life Sciences and School of Medicine, Tsinghua University, Beijing 100084, China
*Correspondence: shi-lab@tsinghua.edu.cn
http://dx.doi.org/10.1016/j.cell.2014.10.051

Since determination of the myoglobin structure in 1957, X-ray crystallography, as the anchoring tool of structural biology, has played an instrumental role in deciphering the secrets of life. Knowledge gained through X-ray crystallography has fundamentally advanced our views on cellular processes and greatly facilitated development of modern medicine. In this brief narrative, I describe my personal understanding of the evolution of structural biology through X-ray crystallography—using as examples mechanistic understanding of protein kinases and integral membrane proteins—and comment on the impact of technological development and outlook of X-ray crystallography.

Brief History

When Wilhelm Roentgen discovered X-ray in 1895, he could not have imagined the powerful applications of X-ray diffraction on crystals of biological samples. Max von Laue showed X-ray diffraction pattern of crystals in 1912, and William Lawrence Bragg derived a general equation, known as the Bragg's Law, to describe the founding principle of image formation by X-ray diffraction (Bragg, 1913) (Figure 1). James Sumner obtained the first crystal of jack bean urease in 1926 and showed the enzyme to be a protein (Figure 1). Max Perutz and John Kendrew decided to pursue crystal structures of proteins—hemoglobin and myoglobin—beginning in the 1940s at the Cavendish Laboratory, University of Cambridge. Their pioneering effort was encouraged by William Lawrence Bragg, who served as the Director of the Cavendish Laboratory between 1938 and 1954. In 1953, James Watson and Francis Crick, both employed at the Cavendish Laboratory, deduced a DNA double-helix model on the basis of X-ray fiber diffraction images of DNA generated by Rosalind Franklin (Watson and Crick, 1953).

The entire biological research community was both excited and shocked to see the very first crystal structure of a macromolecule in 1957—that of sperm whale myoglobin by John Kendrew (Kendrew et al., 1958). The structure of myoglobin, initially determined at 6 Å resolution but quickly improved to 2 Å (Kendrew et al., 1960), confirmed the α-helical conformation as proposed by Linus Pauling and Robert Corey (Pauling and Corey, 1951a, 1951b, 1951c; Pauling et al., 1951). Kendrew's success in structure determination of myoglobin was indispensably assisted by Perutz' solution to the phase problem—multiple isomorphous replacement through heavy atom soaks. Max Perutz presented his own X-ray structure on the larger protein hemoglobin at 5.5 Å (Perutz et al., 1960) and took a few years to improve the resolution to 2.8 Å (Perutz et al., 1968a, 1968b). Kendrew founded the *Journal of Molecular Biology* and served as Editor-in-Chief for a number of years. Kendrew also helped establish the European Molecular Biology Laboratory in Heidelberg and became its founding director. Perutz, on the other hand, founded and directed the MRC Laboratory of Molecular Biology (Figure 1). Notably, the double-helix structure of DNA was finally visualized in 1980 by the X-ray structure of a 12-base-pair palindromic DNA, known as the Dickerson dodecamer (Wing et al., 1980).

DNA is the genetic material of almost all living matters, and proteins are the engines of life. Structural elucidation of DNA and protein is arguably the most important scientific discovery in the 20th century. Proposal of the double-helix structure of DNA has fundamentally changed our perception of life and has ushered in a new era of modern biology. Crystal structures of myoglobin and hemoglobin allowed us to link protein function to its chemical details. In many respects, the atomic details offered by X-ray crystallography allowed mechanistic understanding of protein function, which marks the beginning of molecular biology. Kendrew and Perutz have been fondly named fathers of molecular biology.

Early crystallographic studies focused on abundant proteins, most often enzymes, from animal organs and tissues. Following the successes on myoglobin and hemoglobin, structural information was obtained for at least seven additional proteins in the 1960s, including the first enzyme hen egg white lysozyme (Blake et al., 1965), ribonucleases A and S (Kartha et al., 1967; Wyckoff et al., 1967), chymotrypsin (Matthews et al., 1967), papain (Drenth et al., 1968), carboxypeptidase A (Lipscomb et al., 1969), and subtilisin (Wright et al., 1969). These structures, together with those of many other enzymes in the 1970s and beyond, reveal the active site conformations and catalytic mechanisms, which form the physical basis of molecular enzymology.

The Protein Data Bank (PDB), a central repository for three-dimensional structural data of macromolecules, was established in 1971 at the Brookhaven National Laboratory with seven initial entries. As of August 26, 2014, there were 102,863 total entries in the PDB, of which 88.7% were determined by X-ray crystallography, 10.3% by nuclear magnetic resonance (NMR), and 0.8% by electron microscopy (EM) (Figure 2A). Following structure determination of the lysozyme from bacteriophage T4 (T4 lysozyme) (Matthews and Remington, 1974), it became a paradigm

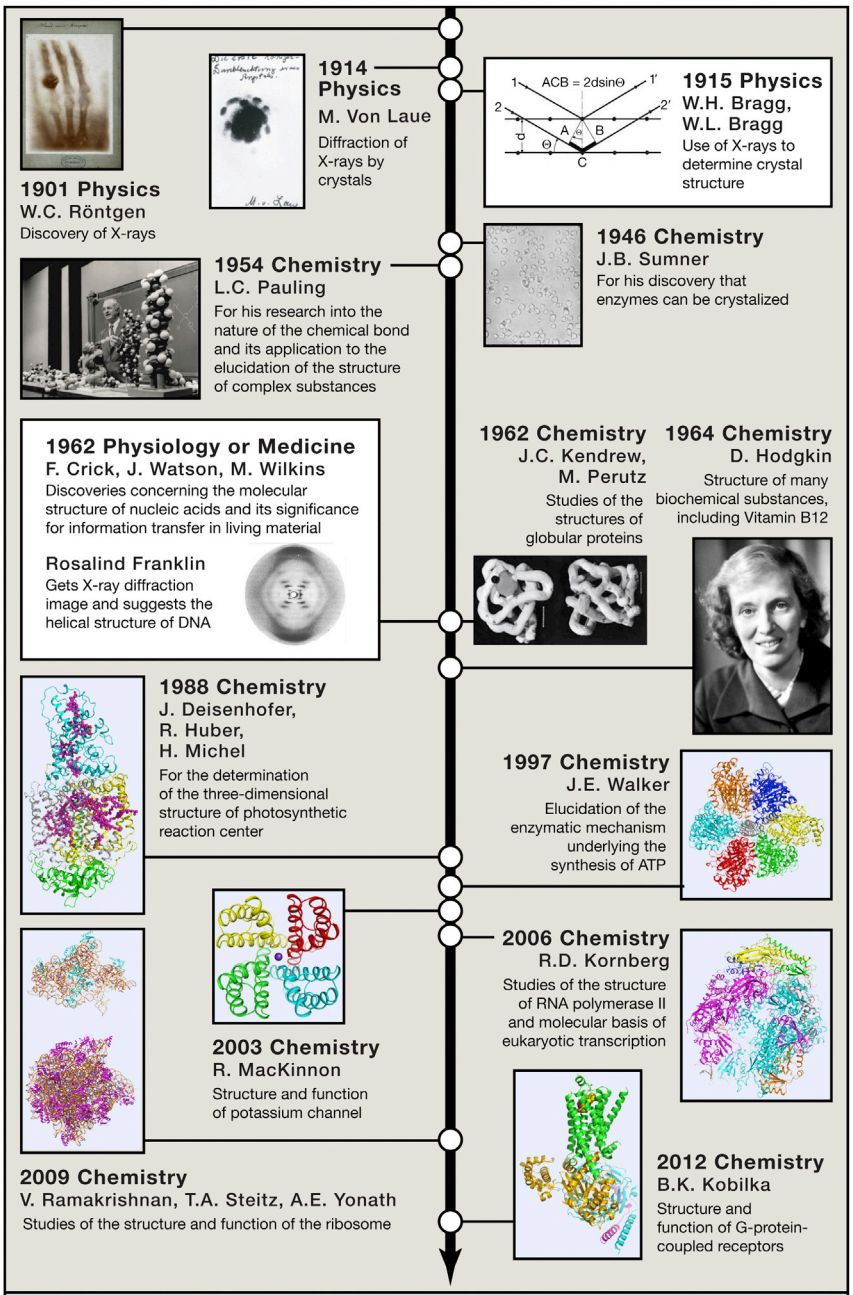

1917	Physics	C.G. Barkla	Discovery of the characteristic Röntgen radiation of the elements
1929	Physics	L.-V. de Broglie	The wave nature of the electron
1936	Chemistry	P.J.W. Debye	For his contributions to our knowledge of molecular structure through his investigations on dipole moments and on the diffraction of X-rays and electrons by crystals
1937	Physics	C.J. Davisson G. Thompson	Diffraction of electrons by crystals
1972	Chemistry	C.B. Anfinsen	Folding of protein chains
1982	Chemistry	A. Klug	Development of crystallographic electron microscopy and discovery of the structure of biologically important nucleic acid-protein complexes
1985	Chemistry	H. Hauptman J. Karle	Development of direct methods for the determination of crystal structures
1994	Physics	C. Shull, N. Brockhouse	Neutron diffraction
2013	Chemistry	M. Karplus, M. Levitt, A. Warshel	Development of multiscale models for complex chemical systems

Figure 1. The History of X-Ray Crystallography in the Eyes of Nobel Prizes

Major achievements in the development and application of X-ray crystallography have been recognized by at least 14 Nobel Prizes. The first Nobel Prize in physics was awarded to Roentgen in 1901 for his discovery of X-rays. The next two Nobel Prizes in 1914 and 1915 were given to Laue for his discovery of X-ray diffraction by crystals and to the Bragg father and son for the use of X-rays to determine crystal structure. Sumner was awarded a Chemistry Prize in 1946 for crystallization of the enzyme urease. Pauling won a Chemistry Prize in 1954 for his research into the nature of chemical bond and its application in structure determination. The year 1962 was quite special, with the Chemistry Prize awarded to Kendrew and Perutz for their pioneering work in protein structure determination, and the Physiology or Medicine Prize bestowed on Crick, Watson, and Wilkins for their contribution in the discovery of DNA structure. Hodgkin was awarded a Chemistry Prize in 1964 for structural elucidation of many biochemical substances, including vitamin B12. The next six Nobel Prizes were awarded to macromolecular crystallographers: Deisenhofer, Huber, and Michel in 1988 for the structure of bacterial photosynthetic reaction center; Walker in 1997 for the structure of F1-ATPase; MacKinnon in 2003 for potassium channels; Kornberg in 2006 for the structure of RNA polymerases; Ramakrishnan, Steitz, and Yonath in 2009 for the structure of ribosome; and Kobilka in 2012 for the structure of GPCR. Listed in the lower left corner are nine Nobel Prizes that are closely related to X-ray crystallography.

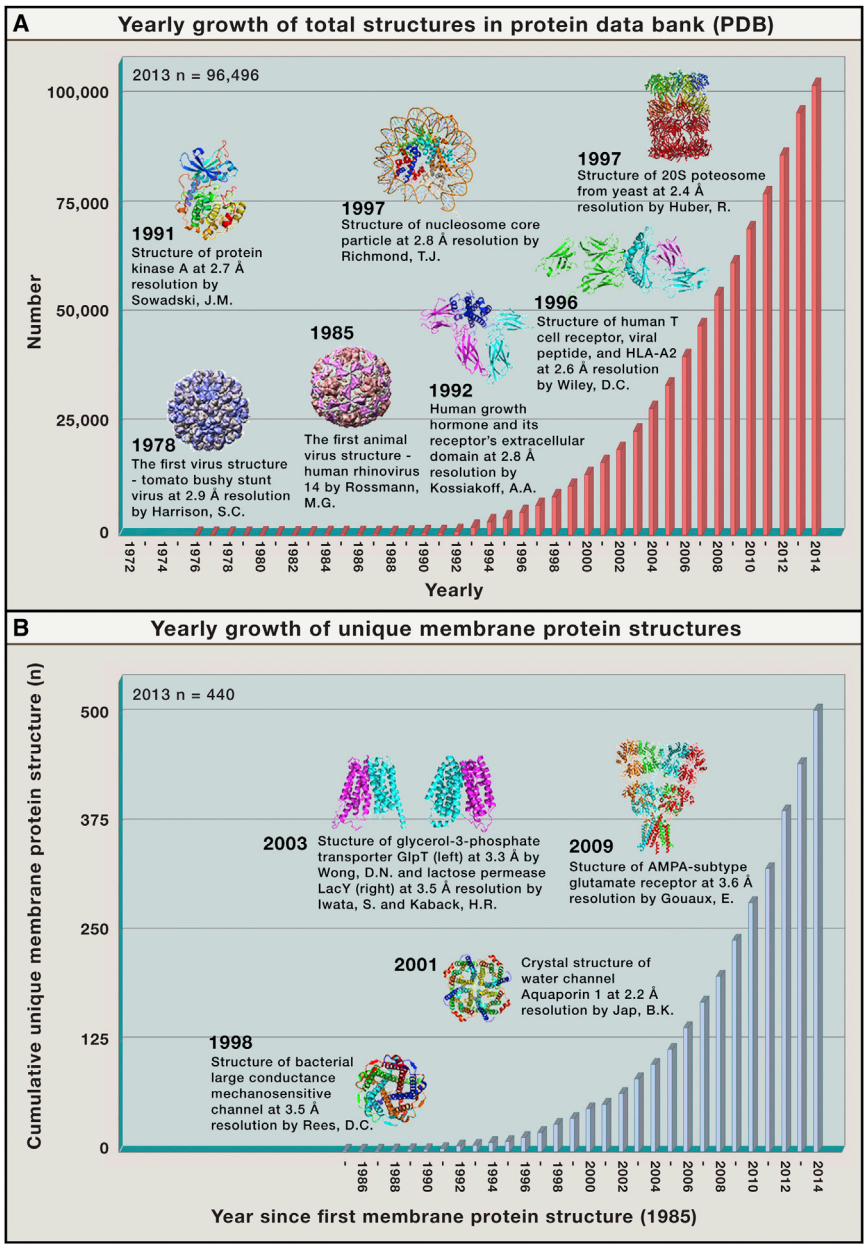

Figure 2. Entries in the Protein Data Bank Have Enjoyed Near-Exponential Growth in the Past 30 Years

(A) The total number of entries of PDB. The PDB was established in 1971 at the Brookhaven National Laboratory with only seven entries. The total number of entries grew to 69 in 1980, 507 in 1990, 13,597 in 2000, and 70,039 in 2010. As of August 26, 2014, there were 102,863 total entries in the PDB, of which 88.7% were determined by X-ray crystallography, 10.3% by NMR, and 0.8% by EM. Some of the representative X-ray structures are indicated in the chart.

(B) The total number of unique membrane protein structures in PDB. In sharp contrast to their heavy presence, structures of membrane proteins only account for just over 1% of all entries in the PDB, with 1,520 total entries and 499 unique structures as of August 31, 2014 (http://blanco.biomol.uci.edu/mpstruc/).

for the study of protein folding and thermodynamics (Baase et al., 2010). In addition to the study of enzymes, viruses became hotly pursued in the 1960s and 1970s. Following his pioneering research into the tomato bushy stunt virus (Harrison, 1969; Harrison and Jack, 1975), Stephen Harrison and colleagues reported the first virus structure at an atomic resolution of 2.9 Å, revealing 180 copies of the capsid protein arranged in an icosahedral particle (Harrison et al., 1978) (Figure 2A). Aaron Klug and colleagues solved the X-ray structure of the TMV protein disk at 2.8 Å resolution (Bloomer et al., 1978) and obtained a low-resolution structure of nucleosome core particle (Finch et al., 1977; Richmond et al., 1984).

Two exciting developments in biology—discovery of gene regulation in the 1960s and emergence of recombinant DNA technology in the late 1970s—raised the question of how DNA sequences could be specifically recognized by transcription factors. Seeking an answer to this question became an important theme for structural biology in the 1980s (for more details, please see Cramer [2014] in this issue of *Cell*). Many DNA-binding motifs were identified, and a number of crystal structures of protein-DNA complexes were elucidated (Aggarwal et al., 1988; Anderson et al., 1987; Otwinowski et al., 1988; Wolberger et al., 1988). There were many other exciting developments in the 1980s. Michael Rossmann's group determined the first atomic resolution crystal structure of a human common cold virus (Rossmann et al., 1985) (Figure 2A). These early findings were followed up with a barrage of structural information on viruses, including mengo virus (Luo et al., 1987) and foot-and-mouth disease virus (Acharya et al., 1989). Due to impending health threats, disease-causing viruses continue to attract ample attention from the structural biology community. Insights gained from these virus structures have, in turn, revolutionized our concepts of virology and helped vaccine design and drug discovery. The 1980s also marks the beginning of structural biology on integral membrane proteins, with determination of atomic resolution X-ray structures of the bacterial photosynthetic reaction center (Allen et al., 1987; Deisenhofer et al., 1985).

Compared to the 1980s, paces of structural biology were considerably faster in the 1990s. The total number of PDB entries increased from less than 400 at the beginning of the year 1990 to more than 13,000 by the end of the year 2000 (Figure 2A). Cellular signal transduction was the principal focus of biological investigation in the 1990s; consequently, the central theme of structural biology during this period was mechanistic understanding of cell

signaling. Crystal structures were elucidated for numerous signaling motifs, exemplified by the phosphotyrosine recognition SH2 domain (Waksman et al., 1992), the phosphoinositol-binding PH domain (Ferguson et al., 1995), the proline-rich sequence binding SH3 domain (Musacchio et al., 1992, 1994), and the carboxyl-terminal peptide-binding PDZ domain (Doyle et al., 1996). The modular nature of these motifs and characterization of their binding specificities constitute an important basis for the development of synthetic biology and chemical biology.

Signal transduction often begins in the extracellular space with ligand binding to its cell-surface receptor. Crystal structure of the complex between human growth hormone and the extracellular domain of its receptor revealed a single hormone molecule recognized by two molecules of receptor (de Vos et al., 1992) (Figure 2A). Some of the other early cocrystal structures include the extracellular domain of TNF receptor bound to TNF-β (Banner et al., 1993), the extracellular fragment of interferon-γ receptor bound to interferon-γ (Walter et al., 1995), and domain 2 of the Flt-1 receptor bound to VEGF (Wiesmann et al., 1997). These ligand-receptor structures give rise to the principle that receptor clustering induced by ligand binding serves as a platform for signaling, which usually involves phosphorylation by receptor kinases. Crystal structure of the catalytic subunit of protein kinase A (PKA)—the first for a protein kinase—revealed an amino-terminal lobe rich in β strands and a carboxyl-terminal lobe with mostly α helices (Knighton et al., 1991) (Figure 2A). The kinase fold observed in PKA was soon confirmed by dozens of crystal structures of other important protein kinases in the 1990s. Understanding of immune signaling by the T cell receptor (TCR) is markedly enhanced by structures of TCR and their complexes with MHC-peptide antigens (Garboczi et al., 1996; Garcia et al., 1996) (Figure 2A).

Structural biology of membrane proteins enjoyed rapid development in the 1990s and beyond. As an extension of X-ray crystallography, electron crystallography was successfully applied to determine the structure of membrane proteins that formed two-dimensional crystals at low resolution in the 1980s and near-atomic resolution in the 1990s. Following two decades of method development on electron crystallography (Subramaniam et al., 2002), Richard Henderson and colleagues succeeded in the elucidation of a 3.5 Å resolution structure of bacteriorhodopsin using electron diffraction data (Grigorieff et al., 1996). Kühlbrandt and colleagues generated a 3.4 Å resolution structure of a plant light-harvesting complex (Kühlbrandt et al., 1994). A striking 1.9 Å resolution was achieved for two-dimensional aquaporin-0 crystals, which allowed clear visualization of lipid-protein interactions (Gonen et al., 2005).

X-ray structure of the mitochondrial F1-ATPase at 2.8 Å resolution revealed distinct conformations for the three catalytic β subunits (Abrahams et al., 1994). Structural analysis of a bacterial potassium channel—the first structure of a recombinant integral membrane protein—provided insights into potassium conduction and selectivity (Doyle et al., 1998). This work was followed up with systematic structural studies of potassium channels, which offer molecular explanations for gating of the ion-conducting pore (MacKinnon, 2003). X-ray structure of the bacterial large-conductance mechanosensitive channel (MscL) revealed a homopentameric assembly and served as a foundation for understanding other mechanosensitive channels (Chang et al., 1998) (Figure 2B). Structural analysis of the water channel aquaporin-1 identified a tetrameric assembly with water molecules localized along a selectivity filter (Figure 2B) (Sui et al., 2001). Crystal structure of the AMPA-type GluA2 receptor revealed a 2-fold symmetry in the extracellular domain and a 4-fold symmetry in the membrane-spanning ion channel domain (Sobolevsky et al., 2009). The first crystal structures on recombinant membrane transporters were elucidated for the lactose permease LacY (Abramson et al., 2003) and the glycerol-3-phosphate transporter GlpT (Huang et al., 2003), defining a conserved fold for the major facilitator superfamily (MFS) of secondary active transporters (Figure 2B). Crystal structure of the human glucose transporter GLUT1—the first eukaryotic MFS structure—allows rationalization of disease-derived mutations (Deng et al., 2014). Following an early X-ray structure on bovine rhodopsin (Palczewski et al., 2000), crystal structures of the recombinant G-protein-coupled receptor (GPCR) were reported on β2 adrenergic receptor (Cherezov et al., 2007; Rasmussen et al., 2007). Structure of an agonist-bound β2 adrenergic receptor in complex with a nucleotide-free Gs heterotrimer provided a preliminary answer to how ligand binding to GPCR triggers the activation of G protein in the cytoplasm (Rasmussen et al., 2011).

Improvement of hardware and software in X-ray crystallography has greatly accelerated the pace of discovery and emboldened structural biologists to attack challenging research projects. Structural elucidation of the proteasomal 20S particles revealed the architecture and identified the proteolytic mechanisms (Groll et al., 1997; Löwe et al., 1995; Seemüller et al., 1995) (Figure 2A). Crystal structure of the GroES-GroEL complex markedly improved our understanding of chaperone-assisted protein folding (Xu et al., 1997b), whereas structural analysis of the nucleosome core particle shows in atomic detail how 146 base pairs of DNA are assembled around the histone octamer (Luger et al., 1997) (Figure 2A). Crystal structure of the large ribosomal subunit, including 2833 RNA nucleotides and 27 proteins, was determined at an atomic resolution of 2.4 Å (Ban et al., 2000) and expanded our protein-RNA recognition database as of the year 2000 by a factor of 6-fold. Since the early 1990s, biologically important megacomplexes and macromolecular assemblies have represented increasingly attractive targets for structural biologists. X-ray structures of the eukaryotic exosomes have revealed important insights into the degradation and processing of cellular RNA (Bonneau et al., 2009; Liu et al., 2006; Makino et al., 2013; Wasmuth et al., 2014). Preliminary structural analysis of the U1, U4, and U6 snRNPs, three subcomplexes of the eukaryotic spliceosome, provided mechanistic insights into mRNA slicing (Leung et al., 2011; Montemayor et al., 2014; Pomeranz Krummel et al., 2009; Zhou et al., 2014). Crystal structure of the human COP9 signalosome revealed molecular architecture of the eight-subunit complex (Lingaraju et al., 2014). The combination of X-ray crystallography with single-particle cryo-EM analysis has been routinely used to provide accurate information on megacomplexes, as exemplified by structure of the yeast 26S proteasome (Beck et al., 2012).

The vast amount of information in the PDB serves as the structural basis for understanding biology and innovating medicine.

X-ray crystallography as a tool has played a dominant role in the past five decades in deciphering the molecular mechanisms of virtually all biological processes. It is truly a mission impossible to attempt coverage of, even if just glossing over, all major achievements of structural biology. Because this narrative is targeted to a general readership, the goal is to showcase the spirit of structural biology through brief description of representative examples—how X-ray crystallography has helped transform the understanding of biology. Therefore, I will mainly comment on two areas of biological research that have been galvanized by X-ray crystallography: kinase regulation and membrane protein structure-function relationship (for the areas of chromatin and transcription, please see Cramer [2014] in this issue of *Cell*). Within each research area, the focus is not to provide a comprehensive review but to discuss pioneering structural investigation and select follow-up studies.

Kinases and Anticancer Drugs

cAMP-Dependent PKA

Reversible protein phosphorylation was discovered on glycogen phosphorylase in the 1950s by Edwin Krebs, Edward Fischer, Earl Sutherland, and Wosilait (Fischer and Krebs, 1955; Sutherland and Wosilait, 1955). The first essential step in glycogen metabolism—its phosphorylation—is mediated by glycogen phosphorylase, whose activation depends on phosphorylase kinase. The conversion of inactive phosphorylase kinase to its activated form is mediated by phosphorylase kinase kinase, also known as cyclic AMP (cAMP)-dependent protein kinase, or PKA. The catalytic subunit of PKA in its free form is catalytically active; however, two molecules of the catalytic subunits are constitutively bound and inhibited by a homodimer of regulatory subunits. Binding of the second messenger cAMP to the regulatory subunits results in the dissociation and hence activation of the PKA catalytic subunits.

Human genome is predicted to encode 518 putative protein kinases, which, on the basis of substrate specificity, are classified into 90 tyrosine kinases (PTKs) and 428 serine/threonine kinases (PSKs). These kinases play an essential role in virtually all cellular processes. The very first atomic view on any protein kinase was provided in 1991 by the crystal structure of the catalytic subunit of PKA (Knighton et al., 1991). This structure reveals a general architecture of two lobes, with the substrate-binding site and the ATP-binding pocket both located between the two lobes (Figure 3A). An activation helix (αC), which contains a catalytic triad residue, and an activation loop, whose phosphorylation results in the activation of the kinase, are positioned next to the hinge between the two lobes. These structural features become the hallmarks of nearly all protein kinases.

Structures of the catalytic subunit of PKA explain substrate specificity and define conformational flexibility (Knighton et al., 1991). Structural analysis of the regulatory subunit reveals mechanism of cAMP recognition (Su et al., 1995). Subsequent structural analysis of PKA with both catalytic and regulatory subunits provides a molecular explanation for the inhibition of PKA and identifies a model for cAMP-mediated activation through binding to the regulatory subunit (Figure 3B) (Kim et al., 2005; Wu et al., 2007). A 2.3-Å X-ray structure of the intact, tetrameric PKA holoenzyme yields insights into allosteric regulation and has ramifications for understanding the regulation of other conserved kinases (Figure 3C) (Zhang et al., 2012).

Cyclin-Dependent Kinases

The temporal-spatial activities of cyclin-dependent kinases (CDKs) determine the fate of the cell cycle and thus are subject to complex regulation. Unlike most kinases, which are active in their free forms, free CDKs are inactive and only attain a basal level of catalytic activity upon association with cyclin. The basal activity can be greatly stimulated by phosphorylation of the activation loop (also known as T loop). The Cip/Kip family of cell-cycle inhibitors, exemplified by p27, potently inhibits the kinase activity of the assembled cyclin-CDK complexes, whereas members of the INK4 inhibitor family can bind the inactive, free CDK, thus preventing its activation. The INK4 inhibitors, exemplified by p16INK4a, also bind and inhibit active cyclin-CDK complexes.

Crystal structure of free CDK2 reveals a misaligned conformation for the activation helix (PSTAIRE helix) and the T loop, providing an immediate explanation to the lack of catalytic activity for the free kinase (De Bondt et al., 1993). Binding by cyclin A induces large conformational changes in the PSTAIRE helix and T loop, resulting in correct alignment of the active site residues and opening of the catalytic cleft (Jeffrey et al., 1995). Phosphorylation of CDK2 in the T loop results in the reorganization of the local structural elements, priming it for substrate binding (Russo et al., 1996b). Remarkably, the inhibitory domain of $p27^{Kip1}$ adopts an extended conformation to interact with both cyclin A and CDK2, with an invariant residue inserting into the catalytic cleft of CDK2 and displacing ATP (Russo et al., 1996a). By contrast, the INK4 inhibitors $p16^{INK4a}$ and $p19^{INK4d}$ bind close to the ATP-binding site of CDK6 and cause structural changes in the catalytic cleft to negatively affect the kinase activity (Brotherton et al., 1998; Russo et al., 1998). The binding site for $p16^{INK4a}$ or $p19^{INK4d}$ is opposite of where cyclin binds, explaining why the INK4 inhibitors can bind both free and cyclin-bound CDKs.

Advent of structural information on CDKs greatly facilitated the screening and design of specific small-molecule inhibitors that block their kinase activities. These inhibitors, mostly ATP analogs, effectively stopped cancer cell growth in petri dish and in animal models. The outcome of anticancer clinical trials thus far has been less than desirable, with notable toxicity and marginal efficacy. For example, flavopiridol exhibited multifaceted, antiproliferative effects in preclinical research but had disappointing performance in clinical trials with narrow therapeutic window and off-target effects. The more selective, second generation CDK inhibitor dinaciclib has entered phase III clinical trial. A notable advance is the development of palbociclib, a highly selective inhibitor of CDK4 and CDK6, for treatment of the HER2−/ER+ breast cancer. In addition, the problem of cross-reactivity by ATP analogs can be effectively dealt with by the development of inhibitors that target sites other than the ATP-binding pocket (Abate et al., 2013).

BCR-ABL, EGFR, and Other Kinase Targets

BCR-ABL is the fusion product of chromosome translocation—a portion of the *Bcr* gene on chromosome 22 is fused to the *Abl* tyrosine kinase gene on chromosome 9 in the Philadelphia chromosome. BCR-ABL is constitutively activated and drives the development of chronic myelogenous leukemia (CML). Perhaps

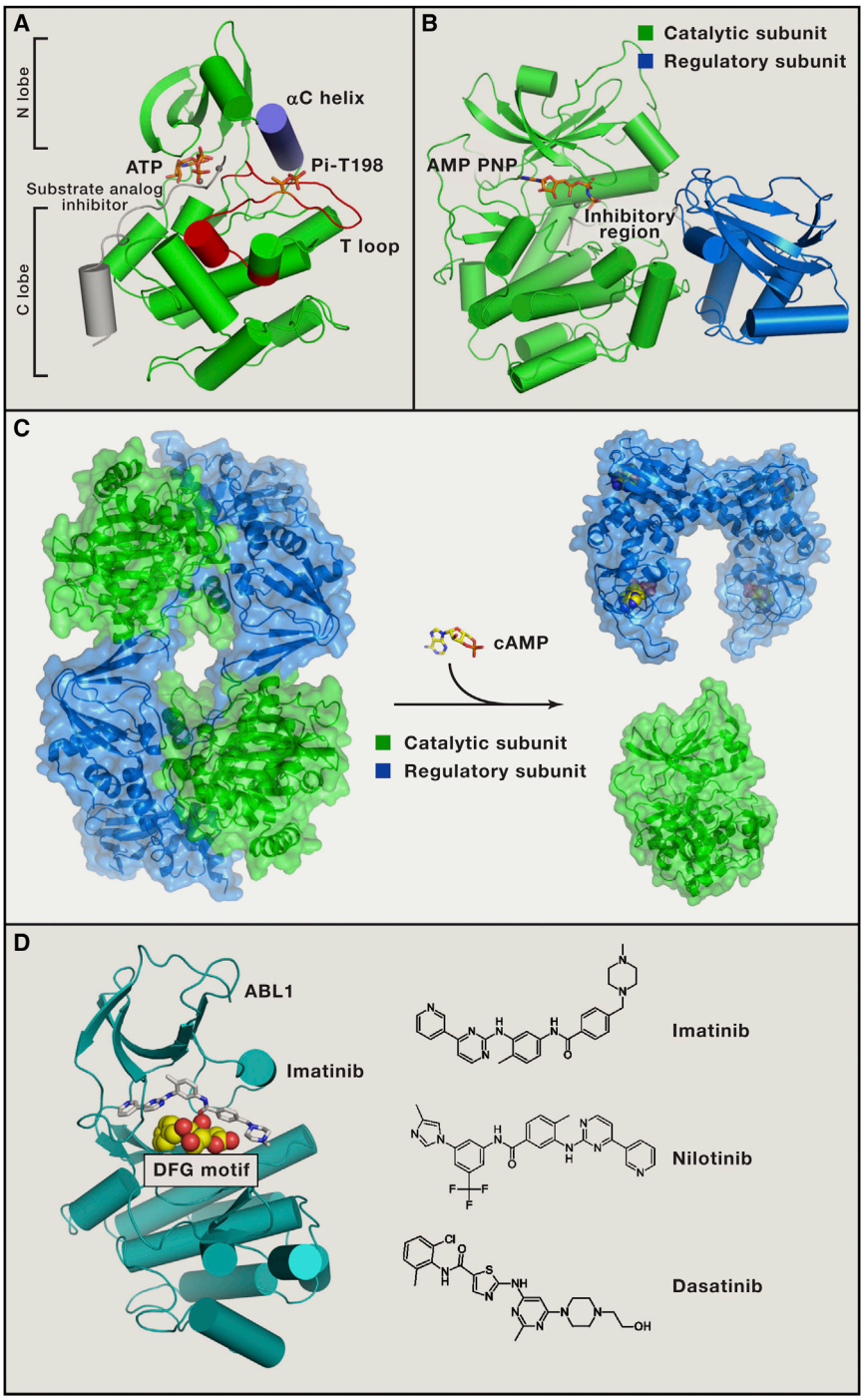

Figure 3. Kinase Structure, Regulation, and Inhibitors

(A) Crystal structure of the catalytic subunit of protein kinase A (PKA, PDB code 1ATP, colored green). The activation helix (αC helix) in the N lobe is colored purple, and the activation loop (T loop) is highlighted in red. ATP and phosphothreonine 198 (Thr198) in the T loop are indicated. The substrate analog inhibitor is represented in gray.

(B) Crystal structure of the complex between PKA catalytic subunit and regulatory subunit (PDB code 3FHI). The PKA catalytic and regulatory subunits are colored green and blue, respectively. The ATP analog AMP-PNP is shown in sticks. The inhibitory region of the regulatory subunit is represented in gray.

(C) Mechanism of cAMP-mediated activation of PKA. In the absence of cAMP, two catalytic subunits (green) and two regulatory subunits (blue) assemble into an inactive, tetrameric PKA holoenzyme (PDB code 3NTP). The binding of cAMP to the regulatory subunits causes pronounced conformational changes, leading to dissociation of the catalytic subunits and producing a dimeric cAMP-bound regulatory subunits (PDB code 4MX3) and two free active catalytic subunits (PDB code 1ATP).

(D) Small-molecule inhibitors of BCR-ABL as potent anticancer drugs. Crystal structure of the human ABL1 kinase domain bound to the anticancer drug imatinib (PDB code 2HYY) is shown in the left panel. Imatinib is a potent drug targeting CML through binding and inhibition of BCR-ABL. Two other inhibitors, nilotinib and dasatinib, are used to treat CML patients with imatinib-resistant mutations. The three small molecule inhibitors are shown in the right panel.

the most celebrated, anticancer kinase inhibitor is imatinib, also known as gleevec or STI-571, which targets BCR-ABL (Shah and Sawyers, 2003). Nearly all chronic myelogenous leukemia (CML) patients who took the drug in the first phase I trial in 1998 were responding; imatinib was approved by FDA in 2001. Imatinib also potently inhibits the tyrosine kinases c-kit and PDGFR, and its clinical use has been approved for a few other cancer types associated with c-kit or PDGFR activation. Crystal structures reveal the precise interactions of an imatinib variant with surrounding residues in the ATP-binding pocket of BCR-ABL and explain how patient-derived mutations (such as T315I) inactivate imatinib binding (Figure 3D) (Nagar et al., 2002; Schindler et al., 2000). Imatinib, classified as a type II kinase inhibitor, binds the kinase in its inactive DFG-out conformation. The structural information guided subsequent development of second-generation inhibitors that stabilize these kinase-specific inactive conformations. These inhibitors include ponatinib, which is effective against the T315I mutation, and nilotinib (sometimes known as super gleevec, Figure 3D), which works well against the majority of CML mutations (except T315I). The structural information also helped design of the type I kinase inhibitors, exemplified by dasatinib (Figure 3D), which bind the kinase in its active DFG-in conformation. These second-generation inhibitors are used to treat relapsed CML patients with imatinib-resistant mutations.

The epidermal growth factor receptor (EGFR) family of receptor tyrosine kinases (RTK) has four members ErbB1–4, each with an extracellular ligand-binding domain, a single transmembrane

segment, and an intracellular kinase domain. The activation mechanism of EGFR has been elegantly revealed by crystallographic discovery and subsequent biochemical analysis (Burgess et al., 2003; Zhang et al., 2006). Growth factor binding induces conformational changes in the extracellular domain, leading to its dimerization with the two ligands on opposite sides of the heterocomplex (Garrett et al., 2002; Ogiso et al., 2002). The EGFR kinase domain exists in an autoinhibited conformation, with key residues Leu834 and Leu837 stabilizing the inactive conformation of the αC helix. Receptor dimerization, induced either by ligand binding or by high protein concentrations during crystallization, facilitates formation of an asymmetric dimer, where the C-lobe of the activator kinase interacts with the N-lobe of the receiver kinase, leading to allosteric activation of the latter (Zhang et al., 2006). The structural observations also provide a satisfying explanation to how mutations of Leu834/Leu837 drive EGFR activation. Aberrant activation of EGFR contributes to the development of a number of malignant cancer types. A few small-molecule inhibitors of EGFR have been used in the clinic to treat cancers, such as gefitinib (popularly known as Iressa) for treating non-small-cell lung cancer (NSCLC). Patients with activating mutations in EGFR respond very well to the treatment of gefitinib (Lynch et al., 2004; Paez et al., 2004). Other small-molecule inhibitors targeting EGFR include lapatinib for breast cancer and erlotinib (or Tarceva) for NSCLC and pancreatic cancer.

Monoclonal antibodies have also been developed to prevent ligand binding to EGFRs or to sabotage dimerization of the extracellular domain. Herceptin, or trastuzumab, which blocks ligand binding by associating with the extracellular domain of ErbB2/HER2 (Cho et al., 2003), proved to be effective in treating ErbB2-overexpressing breast cancer (Recondo et al., 2014). Pertuzumab, on the other hand, prevents receptor dimerization by binding to the extracellular domain of ErbB2/HER2 (Franklin et al., 2004). Cetuximab, or Erbitux, which prevents both ligand binding and receptor dimerization through binding to domain III of the EGFR extracellular region (Li et al., 2005), has been approved for the treatment of metastatic colon cancer, NSCLC, and head and neck cancer. More recently, monoclonal antibody and cytotoxic small molecule have been combined into a single entity, named antibody-drug conjugates, which directly target cancer cells with high-dose chemotherapy. Trastuzumab emtansine (or Kadcyla) is such an antibody-drug conjugate that combines trastuzumab and the cytotoxic agent mertansine; it is approved to treat HER2-positive metastatic breast cancer (Recondo et al., 2014).

Chemical Genetics of Protein Kinases

The structural information not only facilitated drug discovery targeting various malignancies but also gave birth to chemical genetics on kinases. The proto-oncogene c-Src, discovered by J. Michael Bishop and Harold Varmus, exists in normal cells in an inactive conformation. In the crystals of autoinhibited c-Src, the SH3 domain, the SH2 domain, and the kinase domain interact with each other to assemble into a tightly folded assembly in which the phosphorylated Tyr527 binds to the SH2 domain and locks c-Src in an inactive conformation (Sicheri et al., 1997; Xu et al., 1997a). Activation of the c-Src pathway, triggered by dephosphorylation of Tyr527, contributes to multiple cancer types. On the basis of structural modeling, the ATP-binding site of v-Src was mutated such that the resulting v-Src, but not the wild-type (WT) v-Src, could accept a synthetic ATP analog (Shah et al., 1997). The engineered v-Src displayed similar catalytic efficiency, as well as substrate specificity as the WT v-Src, but allowed direct tracing of v-Src substrates in cells (Shah et al., 1997). This strategy was applied to other Src family members and general protein kinases. The engineered kinases, along with the unique ATP analogs, allowed investigation of important biological questions, such as identification of Cdk1 targets in yeast, selective inhibition of neurotrophin in vivo, and discovery of JNK2 as a positive regulator of c-Jun.

Membrane Protein Structure and Function

Membranes compartmentalize cellular processes and enzymatic reactions, and membrane proteins account for 20%–30% of all human proteins. Structures of membrane proteins, however, only account for just over 1% of all entries in the PDB, with 1,520 total entries and 499 unique structures as of August 31, 2014 (Figure 2B). The structural investigation of membrane proteins had been hampered by the technical challenges of poor recombinant expression, insolubility in aqueous solution, and unruly behavior in detergent solubilized forms. In addition, crystals of membrane protein usually diffract X-rays poorly. Consequently, structural biology of membrane proteins lagged behind that for soluble proteins by two decades.

Early effort focused on endogenous membrane proteins, eliminating the hassles of recombinant expression. Crystal structure of a bacterial photosynthetic reaction center at 3 Å resolution—the first atomic-resolution image of any integral membrane protein—reveals the stunning inner workings usually buried within the membrane (Deisenhofer et al., 1985) (Figure 1). X-ray structure of the F1-ATPase from bovine heart mitochondria, determined at 2.8 Å resolution, captured the three catalytic β subunits in distinct conformations and different states of nucleotide binding (Abrahams et al., 1994) (Figure 1). This structural observation lends critical support to the hypothesis that the three catalytic subunits are at different states of the catalytic cycle at any moment, and rotation of the α3β3 subcomplex relative to the γ subunits results in the interconversion of the states.

Roderick MacKinnon was among the first to use recombinant system to express membrane proteins—potassium channels—for structural studies (Figure 1). Despite similar properties between potassium (K^+) and sodium (Na^+), K^+ channels are at least four orders of magnitude more permeant for K^+ than for Na^+. Crystal structure of the K^+ channel from *Streptomyces lividans* (KcsA) at 3.2 Å resolution revealed the first atomic view of an ion channel (Figure 4A) (Doyle et al., 1998). Tetrameric arrangement of the K^+ selectivity filter and structural features of the pore provide explanations to ion selectivity and conduction (Doyle et al., 1998; Roux and MacKinnon, 1999; Zhou et al., 2001). Only two out of four potential K^+ binding sites are occupied in the selectivity filter, allowing energy minimization and optimization of conduction rate (Morais-Cabral et al., 2001). Subsequent structural and biochemical studies on K^+ channels uncovered mechanistic insights into gating of the ion-conducting pore (Jiang et al., 2002, 2003; Long et al., 2005).

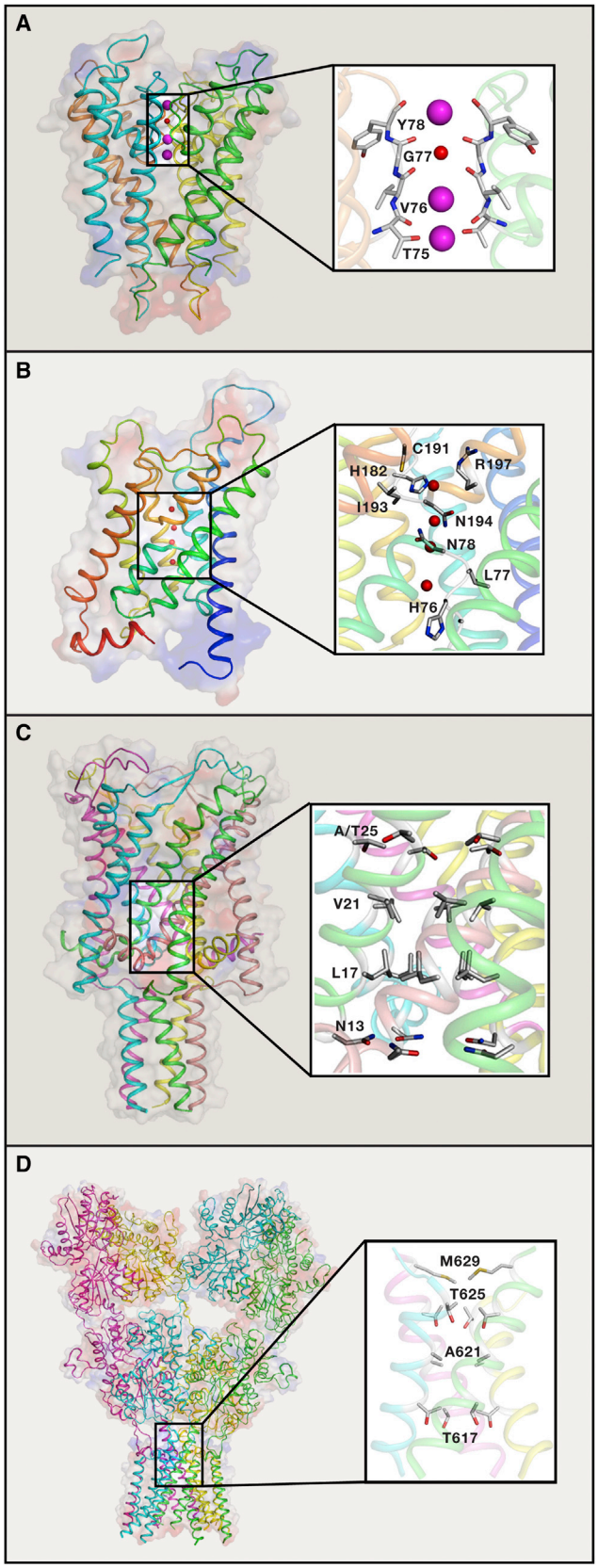

Figure 4. Structures and Mechanisms of Representative Channels

(A) Crystal structure of the potassium channel KcsA (PDB code: 1BL8). KcsA is a homotetramer. Each subunit contains two α helices connected by the pore region, which harbors the selectivity filter. The selectivity filter is shown in a close-up view, with three K^+ ions (magenta spheres) identified. Two K^+ ions are in a rapid equilibrium, with only one of the lower two positions occupied at any instant. One water molecule is shown in red sphere.

(B) Crystal structure of the water channel aquaporin 1 (AQP1) (PDB code: 1J4N). AQP1 is a tetramer with each subunit providing an independent water pore. Four water molecules (red spheres) are located at three hydrophilic nodes along the selectivity filter.

(C) Crystal structure of the mechanosensitive channel MscL (PDB code: 2OAR). MscL is organized as a homopentamer. A water-filled opening from the extracellular side narrows at the cytoplasmic side, where hydrophilic residues may function as the selectivity filter.

(D) Crystal structure of the AMPA-type glutamate receptor GluA2 (PDB code: 3KG2). The GluA2 structure is a homotetramer. In the antagonist-bound structure, the ion channel adopts a closed conformation. Residues forming the narrowest region are indicated in the close-up view.

G-Protein-Coupled Receptors

GPCRs define a large family of seven transmembrane proteins that mediate a wide range of signaling at the plasma membrane. Approximately half of all clinical drugs directly target GPCRs. Working with Robert Lefkowitz, Brian Kobilka cloned and biochemically characterized human α2- and β2-adrenergic receptors (Kobilka et al., 1987a, 1987b, 1988). X-ray structure of bacteriorhodopsin, which bears homology to mammalian GPCR, was determined in 1997 (Pebay-Peyroula et al., 1997), followed by the structure determination of bovine rhodopsin (Palczewski et al., 2000). Conformation of the seven transmembrane helices (TMs) in bovine rhodopsin differs significantly from that in bacteriorhodopsin. Kobilka and colleagues determined the crystal structure of the human β2 adrenergic receptor (β2AR) at 3.4–3.7 Å resolution (Rasmussen et al., 2007). The relatively poor X-ray diffraction of β2AR crystals was successfully mitigated by insertion of T4 lysozyme into the third intracellular loop (Rosenbaum et al., 2007). Crystal structure of the resulting β2AR bound to a diffusible ligand carazolol was determined at 2.4 Å resolution, revealing extensive interactions of carazolol with residues at the ligand-binding site (Cherezov et al., 2007). Structures of activated and/or agonist-bound, as well as antagonist-bound, GPCRs reveal distinct conformations of the ligand-binding pocket. The most notable ligand-induced conformational change on the cytoplasmic side appears to be an outward movement of the cytoplasmic portion of TM5 and TM6. A wealth of rapidly emerging structures on GPCRs has greatly stimulated the interests of major pharmaceutical companies to improve existing drugs and to screening and design new therapeutic modulators.

The principal biological question on GPCR is how conformational changes triggered by ligand binding result in the activation of G protein. A tentative answer to this question was supplied by the crystal structure of an agonist-bound β2AR in complex with a nucleotide-free Gs heterotrimer (Rasmussen et al., 2011) (Figure 1). The most pronounced, agonist-induced conformational change in β2AR is a 14 Å outward movement at the cytoplasmic end of TM6 and TM5. The conformational changes induced by the interactions between β2AR and Gs are propagated to the nucleotide-binding pocket, presumably facilitating replacement of GDP by GTP. The most unanticipated change is a marked displacement of the α-helical domain of Gαs relative to the Ras-like GTPase domain (Rasmussen et al., 2011).

Membrane Transport Proteins

A living cell constantly needs to uptake nutrients from the environment and to expel metabolites and waste materials. This extremely complex process is mediated by a very large number of membrane transport proteins that can be classified into at least four general types: channels or pores, facilitators, secondary active transporters, and primary active transporters. An online database of membrane transport proteins (www.TCDB.org) contains more than 10,000 unique protein sequences that are classified into over 800 transporter families. Membrane proteins of known three-dimensional structure are cataloged online at http://blanco.biomol.uci.edu/mpstruc/. I do not intend to comprehensively cover all known structures of transporters. Rather, I will simply give a few representative examples.

Channels. The aquaporin family of channels, consisting of the water-conducting aquaporins and the glycerol-conducting aquaglyceroporins, plays an essential role in the regulation of cellular osmolarity. Structural analysis of aquaporin-1 (AQP1) revealed a tetrameric assembly and identified four water molecules that are localized at three hydrophilic nodes along an otherwise highly hydrophobic selectivity filter (Figure 4B), supporting rapid water transport (Sui et al., 2001). Subsequent structural analysis of aquaporin Z identified the molecular mechanism for differentiation between water and glycerol by the aquaporin family (Savage et al., 2003). Structure of the glycerol facilitator GlpF revealed an amphipathic selectivity pore that is lined by a number of glycerol molecules in single file (Fu et al., 2000). Structural analysis and molecular dynamics simulation elucidated the molecular mechanism of selective permeability for glycerol (Fu et al., 2000; Tajkhorshid et al., 2002). The aquaporin fold is also observed in other small-molecule transporters such as the pentameric formate channel FocA (Waight et al., 2010; Wang et al., 2009).

Physical forces, in the form of touch, hearing, pressure, and gravity, are primarily sensed by a family of mechanosensitive ion channels, which transduce mechanical strain into an electrochemical response. The X-ray structure of the MscL, determined at 3.5 Å resolution, revealed a homopentamer (Figure 4C) (Chang et al., 1998). In each subunit, a water-filled opening at the extracellular side is followed by a hydrophilic pore that narrows to an occluded region at the cytoplasmic side. This structure serves as a model system for understanding of and comparison with other mechanosensitive channels. Structural analysis of the small-conductance mechanosensitive channel (MscS) shows a heptameric assembly, with the closed-state transmembrane pore connecting to a large chamber in the cytoplasmic side (Bass et al., 2002). Notably, the overall fold in the transmembrane region is different between MscL and MscS, with two TMs in MscL and three TMs in MscS.

Chemical transmitters of excitatory synapses in the central nervous system, exemplified by glutamate, activate receptors on the postsynaptic cells, leading to transmission of signals from one neuron to the next. Ionotropic glutamate receptors (iGluRs) are ligand-gated ion channels. The iGluR family includes AMPA, kainite, and NMDA receptors, which are heterotetrameric or homotetrameric. Crystal structure of the homotetrameric AMPA-type GluA2 receptor bound to a competitive antagonist revealed a closed conformation, with a 2-fold symmetry in the extracellular domain and a 4-fold symmetry in the membrane-spanning ion channel domain (Figure 4D) (Sobolevsky et al., 2009). Structural analysis of the GluA2 receptor allowed proposition of mechanisms for ion channel activation, desensitization, and inhibition by noncompetitive antagonists. These mechanisms were further investigated by the X-ray structure of GluA2 bound to cone snail toxin (Chen et al., 2014) and in distinct functional states (Dürr et al., 2014). Structure of the NMDA-type, heterotetrameric receptor involving two GluN1 and two GluN2B subunits confirmed some of the proposed general mechanisms for iGluRs and provided additional insights (Karakas and Furukawa, 2014; Lee et al., 2014).

Secondary Active Transporters. Unlike channels, transporters never allow simultaneous substrate access from both sides of the lipid membrane. A prevailing model for the general transport mechanism is known as alternating access (Jardetzky, 1966), which postulates that a transporter must switch between at least two conformations: open to the extracellular side (outward-open) for substrate upload and open to the intracellular side (inward-open) for substrate release, or vice versa. Restrained by a series of conformational switches within each transport cycle, a transporter can only move 200–50,000 substrate molecules per second, considerably slower than that for channels (which sometimes can permeate substrates at near diffusion limit). The ability to transport substrate molecules against their concentration gradients, together with the different conformational states within each transport cycle, have made membrane transporters appealing for structural and mechanistic investigations.

The major facilitator superfamily (MFS) transporters are ubiquitously present in all kingdoms of life and play an important role in numerous cellular processes. The first crystal structures on MFS were reported on the lactose permease LacY from *E. coli* (Abramson et al., 2003) and the glycerol-3-phosphate transporter GlpT (Huang et al., 2003) (Figure 5A). The structures revealed a conserved MFS fold of 2-fold symmetric N-domain and C-domain, each comprising six consecutive TMs. The transport path, as well as the substrate-binding site, is located between the N and C domains. The structural information provides immediate explanation to a large body of biochemical and biological observations, particularly on LacY (Kaback, 2005). Distinct conformational states of MFS, which include the multidrug transporter EmrD (Yin et al., 2006), the L-fucose:H^+ symporter FucP (Dang et al., 2010), the peptide transporters $PepT_{So}$ and $PepT_{St}$ (Newstead et al., 2011; Solcan et al., 2012), and the D-xylose:H^+ symporter XylE (Sun et al., 2012) appear to support the alternating access model. Perhaps the best known and most important MFS family members are the glucose transporters GLUT1–4, which are associated with a number of debilitating diseases. Crystal structure of the full-length human GLUT1—the first eukaryotic MFS structure—allows rationalization of disease-derived mutations (Figure 5B) (Deng et al., 2014).

Crystal structure of the sodium:leucine symporter LeuT revealed a conserved fold of ten TMs grouped into two inverted repeats, each containing five consecutive TMs (Figure 5C) (Yamashita et al., 2005). The first TM in each of the two inverted repeats, TM1 or TM6, is discontinuous and contains a highly conserved unwound segment that is positioned in the transport path. A similar fold was subsequently observed in the

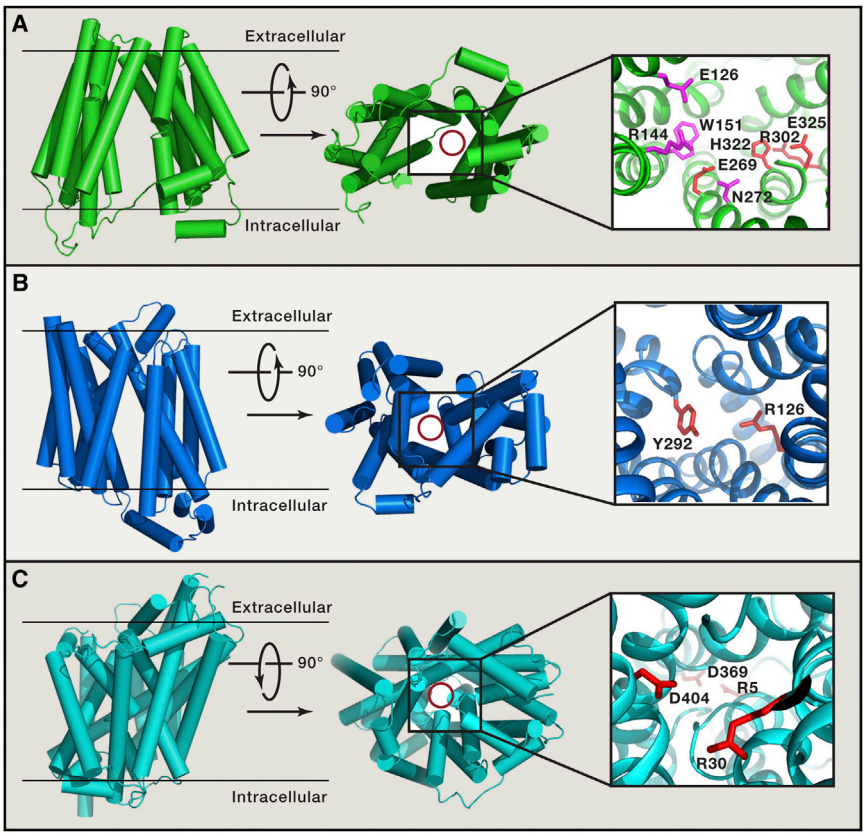

Figure 5. Structures and Mechanisms of Representative Secondary Active Transporters

(A) Crystal structure of the *E. coli* lactose permease LacY. The overall structure of LacY is shown in two perpendicular views (left and middle). The transport path is highlighted by a red circle in the middle panel, and its close-up view is shown in the right panel. Residues involved in substrate binding and proton coupling are colored magenta and red, respectively.

(B) Crystal structure of the human glucose transporter GLUT1. Two amino acids forming the extracellular gate are labeled in the close-up view.

(C) Crystal structure of the sodium symporter LeuT. Arg30 and Asp404 are thought to play a key role at the extracellular gate, whereas Arg5 and Asp369 control the intracellular gate. These four amino acids are indicated in the close-up view.

nucleobase:cation symporter-1 family Mhp1 (Weyand et al., 2008) and the solute sodium symporter family vSGLT (Faham et al., 2008). Remarkably, despite lack of sequence or functional conservation, the same general LeuT fold has been recognized in several membrane transporter families, exemplified by the glycine:betaine transporter BetP (Ressl et al., 2009), and amino acid antiporters AdiC and GadC (Fang et al., 2009; Gao et al., 2009, 2010; Ma et al., 2012). These unanticipated structural findings led to reclassification of membrane transporters, with nine LeuT-fold families now grouped together to constitute the APC superfamily (Saier et al., 2009).

Primary Active Transporters. Primary active transporters, exemplified by the sarco/endoplasmic Ca^{2+}-ATPase (SERCA) and the ATP binding cassette (ABC) transporters, exploit the energy of ATP binding and hydrolysis for substrate transport, usually against concentration gradient of the substrate molecules. The 2.6 Å resolution crystal structure of SERCA1a revealed a complex architecture, with two calcium ions bound in the membrane spanning region (Figure 6A) (Toyoshima et al., 2000). Structural comparison with the enzyme in the absence of calcium suggests large domain movements during active transport, which was confirmed by the structure of SERCA1a in a calcium-free state (Toyoshima and Nomura, 2002). The active transport of calcium ion by this ATPase pump involves several distinct conformation states. These conformational states were visualized by a number of related crystal structures of SERCA, including that bound to ATP or an ATP analog (Olesen et al., 2007; Olesen et al., 2004; Sørensen et al., 2004; Toyoshima and Mizutani, 2004), ADP (Sørensen et al., 2004), and a phosphate analog (Olesen et al., 2007; Toyoshima et al., 2004). Together, these structures allow mechanistic understanding of the complete cycle of calcium transport driven by ATP binding and hydrolysis.

An ABC transporter contains at least four subunits: two transmembrane domains (TMDs) and two ABCs (or nucleotide binding domains, NBDs) located in the cytoplasm. The first crystal structure of the ABC transporter—that of the tetrameric BtuCD complex at 3.2 Å resolution—revealed a central translocation path that is formed between two BtuC subunits within the membrane and closed to the cytoplasmic side by a gate region (Figure 6B) (Locher et al., 2002). This structure serves as a framework for all subsequent structural investigations and mechanistic understanding. Crystal structures, including a bacterial multidrug transporter Sav1866 (Dawson and Locher, 2006), a putative metal-chelate-type transporter (Pinkett et al., 2007), a maltose transporter (Oldham et al., 2007), BtuCD bound to the periplasmic-binding protein BtuF (Hvorup et al., 2007), a bacterial lipid flippase MsbA (Ward et al., 2007), a molybdate/tungstate transporter ModBC (Gerber et al., 2008), and a methionine transporter (Kadaba et al., 2008), captured different conformational and nucleotide-bound states. These snapshots allow proposition of a complete transport cycle for an ABC transporter. The transport cycle is elegantly shown for the maltose transporter MalFGK2, with a number of conformational states observed at atomic details (Chen et al., 2013; Khare et al., 2009; Oldham and Chen, 2011a, 2011b; Oldham et al., 2007).

The energy-coupling factor (ECF) family of membrane transporters shares a similar organization with the ABC transporters with two NBDs and two TMDs. In contrast to the ABC transporters, the two NBDs of an ECF transporter are encoded by two different ATPase genes, and the two transmembrane domains have contrasting roles, with one specific for substrate binding (S component) and the other for energy transduction (T component). Structures of the heterotetrameric ECF

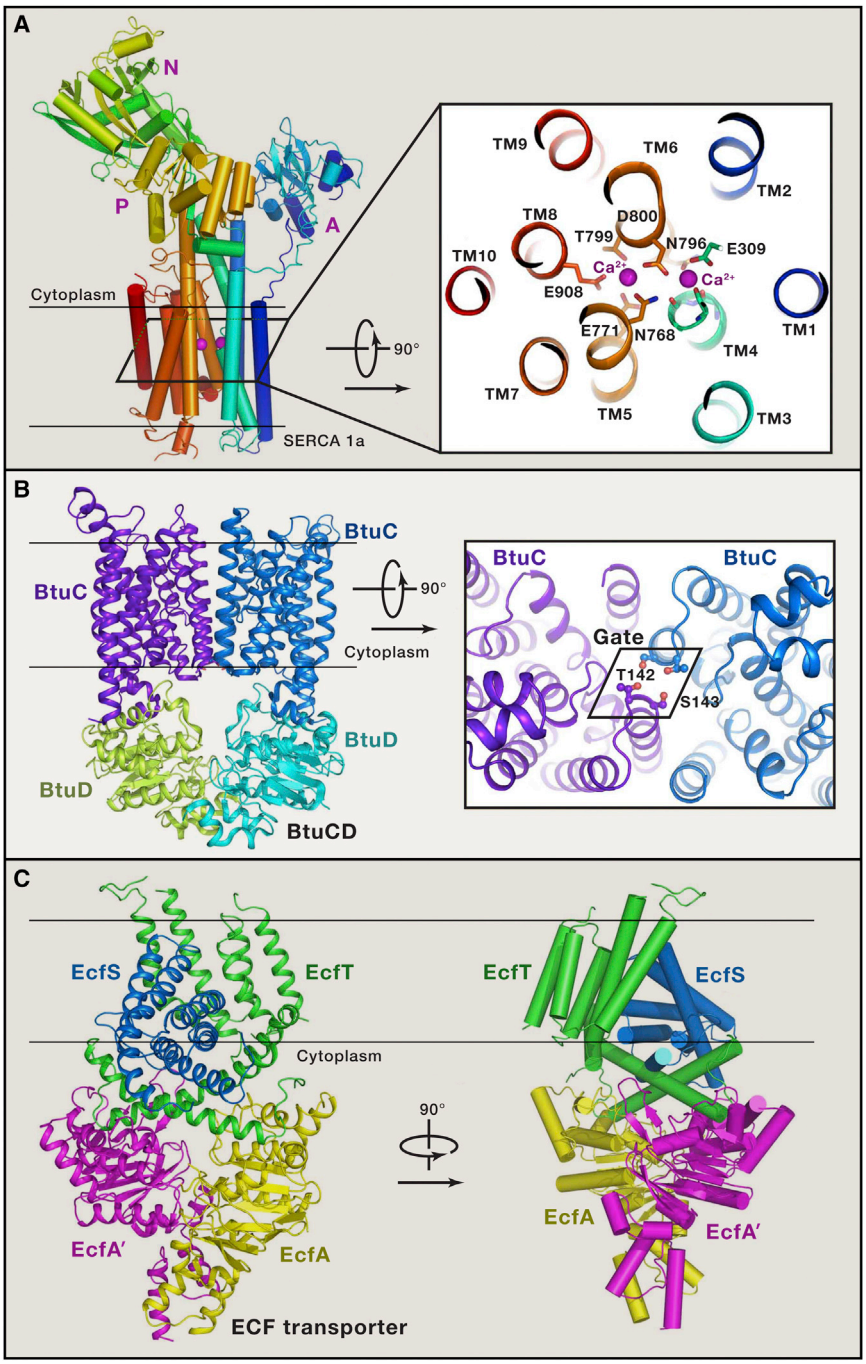

Figure 6. Structures and Mechanisms of Representative Primary Active Transporters

(A) Crystal structure of the calcium ATPase SERCA1a. The structure of SERCA1a is displayed in a rainbow-colored cartoon representation with its amino-terminus in blue and carboxyl-terminus in red (left). Three cytoplasmic domains, A, N, and P, are labeled, and the transmembrane domain consists of ten TMs. The calcium binding sites are shown in a close-up view (right). Two calcium ions are represented in magenta spheres.

(B) Crystal structure of the ABC transporter BtuCD. BtuCD consists of four subunits, two membrane-spanning subunits BtuC (purple and blue), and two ABC subunits BtuD (cyan and green). The transport path is closed to the cytoplasm by a gate region, with two residues Thr142 and Ser143 playing a key role.

(C) Crystal structure of a representative ECF transporter. The structure of a tetrameric ECF transporter is shown in two perpendicular views. The TMs of the substrate-binding S component (EcfS) are nearly parallel to the lipid membrane and perpendicular to those of the energy-transducing T component (EcfT). The structural organization revives the carrier model for membrane transporters.

transporters revealed a striking organization—the six TMs of the S component are placed roughly parallel to the lipid membrane and perpendicular to the TMs of the T component (Figure 6C) (Wang et al., 2013; Xu et al., 2013). These structures, together with results of MD simulation, strongly support the carrier model of substrate transport (Widdas, 1952), which differs from the alternating access model.

Intramembrane Proteases. Regulated intramembrane proteolysis (RIP), which requires cleavage of a membrane-embedded substrate protein by an intramembrane protease within the lipid bilayer, is a universally conserved signaling mechanism from bacteria to human beings (Brown et al., 2000). The most remarkable examples of RIP include cleavage of the cholesterol-controlling transcription factor SREBP by the metalloprotease S2P, the cleavage of the growth factor Spitz by the serine protease rhomboid, and the cleavage of amyloid precursor protein by the aspartate protease presenilin (which is the catalytic component of the γ-secretase). Unlike proteases in aqueous environment, the hydrophilic active site of an intramembrane protease must be accessible to water molecules, which are required for proteolysis, and substrate proteins within the hydrophobic lipid membrane. Structural information is now available on the bacterial homologs of the three classes of intramembrane proteases, including the rhomboid homolog GlpG from *E. coli* (Ben-Shem et al., 2007; Lemieux et al., 2007; Wang et al., 2006; Wu et al., 2006), the archael S2P homolog (Feng et al., 2007), and the presenilin homolog PSH (Li et al., 2013). In all cases, the active site has constant access to water molecules through a funnel that opens either to the extracellular side or the cytoplasmic side. This crystallographic finding is elegantly simple yet completely unanticipated in the absence of structural information. The active site is shielded from the hydrophobic membrane bilayer by one or two gating TMs, which undergo lateral rotation or movement to allow substrate entry. For GlpG, the gating helix TM5 had been captured in fully

open, partially open, and closed conformations. The recent cryo-EM structure of human γ-secretase (Lu et al., 2014), along with the X-ray structure of its putative substrate-recruiting component nicastrin (Xie et al., 2014), revealed tantalizing clues about functional mechanisms of γ-secretase.

Method Development

Protein Expression and Purification

Prior to 1970s, all proteins employed for X-ray crystallography were derived from endogenous sources—mostly animal tissues and organs—and were biochemically purified. These proteins, exemplified by myoglobin and lysozyme, are thermodynamically stable and contain few flexible surface sequences that may hinder crystallization. In late 1970s, discovery of the restriction enzymes greatly facilitated cloning of target cDNA into plasmids, allowing recombinant expression in *E. coli*. Unfortunately, many recombinant proteins, especially those containing multiple domains and/or flexible surface sequences, defied crystallization. Finding a crystallizable protein domain or fragment frequently required multiple trials of protein engineering, each involving different boundaries or mutations for the target protein. Limited proteolysis has been used to identify stable core domains that are amenable for crystallization. One of the most remarkable examples of limited proteolysis was the identification of sequence boundaries for the DNA-binding domain of p53 (Pavletich et al., 1993).

Recombinant coexpression of two or more proteins became a popular strategy in the 1990s. This strategy allowed convenient assembly of multicomponent protein complex. Although bacterial expression is fast and inexpensive, eukaryotic proteins are frequently misfolded or aggregated when expressed in bacteria, likely due to differences in folding environment. Eukaryotic recombinant expression systems, involving yeast, baculovirus-infected insect cells, and mammalian cells, play an increasingly more important role (Assenberg et al., 2013). For mammalian cell expression, both stable cell lines and transient expression through plasmids have succeeded in production of large quantities of materials for crystallization. Stable CHO cells allowed expression and purification of milligram quantity of γ-secretase, a four-component membrane protein complex (Alattia et al., 2013).

Crystallization

Until early 1990s, approximately half of all crystals were generated with ammonium sulfate as the major precipitant in the crystallization buffer. In the year 2013, however, none of the 55 crystal structures reported in the journal *Nature* relied on ammonium sulfate as a crystallization agent. This dramatic change likely reflects the proposition that ammonium sulfate may work better for small protein of greater thermal stability. Perhaps more importantly, the reagents and tools for crystallization have steadily improved in the last two decades, including numerous commercial reagent kits, robotic arms, and development of special methodology for membrane protein crystallization (McPherson and Gavira, 2014). The lipidic cubic phase (LCP) has been widely used for the crystallization of membrane proteins (Caffrey, 2009), with fantastic successes for GPCRs (Cherezov et al., 2010). Bicelles were also applied to membrane protein crystallization (Agah and Faham, 2012).

Although prior experience may facilitate crystallization of a new target protein or macromolecular complex, systematic screening of representative crystallization space is almost always recommended. In all cases of difficult proteins, biochemistry and molecular biology are the keys for crystallization—that is, improvement of solution behavior through biochemical characterization and extensive protein engineering. Insertion of a T4 lysozyme into β2AR proved to be important for improvement of crystal packing and hence X-ray diffraction limit (Rosenbaum et al., 2007). Sequence alignment among homologous proteins frequently yields valuable hints on how to improve the chance of crystallization. For example, replacing five nonconserved amino acids with conserved ones led to crystallization of a presenilin homolog (Li et al., 2013). The crystallization of the AMPA-type receptor GluA2 required carboxyl-terminal and internal deletion, removal of potential glycolysation sites, alanine substitution, and specific mutation (Sobolevsky et al., 2009).

Structure Determination

Since the invention of the oscillation/rotation protocol (Arndt and Wonacott, 1977), it has quickly become the primary X-ray diffraction data collection method on single crystals. Powerful rotating anode generators have been improved continuously to generate X-rays with high intensity. Synchrotron radiation, which supplies X-rays with tunable wavelength and much higher X-ray flux than home source, was brought to the attention of biological crystallographers (Rosenbaum and Holmes, 1971) and quickly became an intimate partner of structural biology. Fast-readout large-area X-ray detectors have been critically important for data collection. Synchrotron beamlines are provided with charge-coupled detectors (CCDs), which make data collection much faster and more accurate than ever before (Phillips et al., 1993). More recently, the concept of shutter-free data collection has been made possible by the pixel array detectors (Pilatus 6M) (Kraft et al., 2009). Cryogenic protection by flash freezing crystals at ~100 K greatly reduced radiation damage (Rodgers, 1994), which allows complete data collection from a single crystal, instead of data merging from multiple crystals in the past.

Software for X-ray data collection and processing, structure determination, and model building has seen major improvements in the last two decades. Most notably, structure determination based on a single crystal became possible with development of the multiwavelength anomalous diffraction (MAD) method (Phillips and Hodgson, 1980; Yang et al., 1990). The ease of selenomethione incorporation into recombinant proteins and the powerful synchrotron radiation have made MAD the preferred method for de novo protein structure determination. Ribonuclease H was the first protein whose structure was successfully determined by selenium-based MAD analysis (Yang et al., 1990). Free R factor, introduced as an objective criteria for structural cross-validation (Brünger, 1992), prevents overrefinement and has quickly become a key parameter for all X-ray structures. Free R factor was also instrumental to implementation of maximum likelihood target functions in crystallographic programs (Pannu and Read, 1996). In 1994, the CCP4 (collaborative computational project, number 4) suite was established, which collected a number of programs for various macromolecular structure determination methods by X-ray crystallography (Collaborative, 1994). Another structure determination package CNS (Brünger et al., 1998),

superseded by PHENIX (Adams et al., 2002), not only provides all necessary programs for X-ray structure solution but also incorporates the refinement method of simulated-annealing after X-plor (Brunger, 1990). Structural genomics demanded high-throughput crystallography, with a number of automated structure solution pipelines established worldwide through integration of existing programs for automation.

The use of MIR demands generation of heavy atom derivatives of the crystals. The heavy atom agents "magic seven" (Boggon and Shapiro, 2000) and "membrane's eleven" (Morth et al., 2006) were recommended for crystals of soluble and membrane proteins, respectively. Polynuclear metal clusters were utilized for phasing of larger protein complexes (Dauter, 2005), exemplified by the ribosomal large subunit (Ban et al., 2000). Compared to heavy metals, bromide or iodine ions can be quickly soaked into protein crystals within minutes. In addition to MIR and MAD, mainstream experimental phasing methods also include single-wavelength anomalous dispersion (SAD), single isomorphous replacement (SIR), multiple isomorphous replacement with anomalous scattering (MIRAS), and single isomorphous replacement with anomalous scattering (SIRAS). Molecular replacement (MR) is used for phasing with a homologous model. Automated model-building algorithms and molecular modeling graphics such as COOT (Emsley and Cowtan, 2004), preceded by O (Jones et al., 1991), have greatly accelerated the pace of structure determination.

Prior to the mid-1990s, it wasn't uncommon for a PhD student in an X-ray crystallography laboratory to spend 3 to 4 years to solve the phase problem, requiring understanding of Patterson maps and resolution of the Harker sections. Consequently, students then usually needed to have certain knowledge of mathematics and physics. Nowadays, a student only needs to mount crystals correctly in the X-ray beam, and the rest—data collection and structure determination—can be just a few clicks away. Intense X-rays at various synchrotron facilities have not only greatly expanded our investigative power on small and weakly diffracting crystals but have also made high-throughput crystallography a reality (Joachimiak, 2009). Remote control of data collection at synchrotrons has eased the trouble of long-distance traveling and sleepless night fatigue.

Hard X-Ray Free Electron Laser

For most X-ray beamlines in existing synchrotrons, destruction of crystals by radiation damage accompanies the process of data collection. Ultrashort (femtoseconds), high-intensity X-ray pulses from free-electron lasers were predicted to provide useful structural information before the destruction of the sample by radiation damage (Neutze et al., 2000). This prediction was reached on the basis of computer simulation of radiation damage, taking into account photon energy, pulse length and intensity, and sample size. A decade later, the proof of concept was established with image construction on diffractions collected on individual virus particles (Seibert et al., 2011) and an electron density map at 8.5 Å resolution of photosystem I, which required millions of nanocrystals and more than 3,000,000 diffraction patterns (Chapman et al., 2011). Both studies were carried out at the Linac Coherent Light Source at Stanford University, which offers the world's first hard X-ray free electron laser (XEFL) with an X-ray intensity of $\sim 10^{12}$ photons in 10 femtoseconds, or about 10–13 orders of magnitude more intense than a regular third-generation synchrotron. The first high-resolution X-ray structure by serial femtosecond crystallography (SFX) was accomplished on lysozyme (Boutet et al., 2012), followed by de novo generation of experimental phases for lysozyme (Barends et al., 2014). This technology has been successfully applied to structure determination of a precursor cathepsin B (Redecke et al., 2013), photosystem II (Kern et al., 2013), and a human serotonin receptor (Liu et al., 2013).

The breathtaking advances of XFEL-based SFX rely on development of container-free sample spraying techniques, with initial crystal hit rate of less than 0.01%. Thus, a vast number of nanocrystals were a prerequisite for such technology, although improvement is underway. By design of the SFX technology, all X-ray diffraction patterns collected are still, partial images, which demand improvements in data processing software (Hattne et al., 2014). The fact of one image per crystal also mandates the isomorphous nature of the microcrystals. These challenges, together with the exceedingly high costs associated with construction of XFEL facility, may qualify the near-future application of SFX to limited pragmatic impact. Nonetheless, as the ultimate technology for determination of macromolecular structure in aqueous solution at room temperature, XFEL is destined to dominate in the future.

Molecular Dynamics

Crystal structures represent static snapshots of macromolecules—averaged temporally and spatially over myriad of subtle conformational differences. In real life, however, these molecules may interconvert among a few distinct conformations to accomplish their biological functions. Thankfully, these distinct conformational states can be trapped by alteration of crystallization condition, inclusion of specific ligand, and/or mutation of specific amino acids. At times of difficulty in capturing one or more of these conformational states, molecular dynamics (MD) simulation came to the rescue. A super machine named Anton extended the timescale of MD simulation to millisecond and therefore enabled the observation of large-scale conformational changes of macromolecules in silico (Lindorff-Larsen et al., 2011; Shaw et al., 2010). Using this approach, the transition between different conformational states was observed for a number of proteins.

In addition to identifying putative conformational changes, MD simulation also helps reveal insights that are sometimes unnoted by structural analysis. Simulation of the c-Src and Hck kinases revealed an important role for the linker sequence between SH3 and SH2 domains, which helps maintain the kinases in an inhibited state (Young et al., 2001). 12 ns MD simulations of the aquaglyceroporin GlpF identified the spatial and temporal probability distribution of a single file of seven to nine water molecules and defined their orientation inside the channel, which mechanistically explained the impermeability of aquaporin to protons (Tajkhorshid et al., 2002). The molecular mechanism of ion selectivity, K^+ versus Na^+, in potassium channels was rationalized by molecular simulation and theoretical computation (Bostick and Brooks, 2007; Noskov et al., 2004).

Time-Resolved X-Ray Crystallography

Conformational dynamics of macromolecules, especially those in enzyme reactions, can be captured by time-resolved X-ray

crystallography, which uses intense, polychromatic X-ray pulses to generate Laue diffraction from a single crystal upon induction of light-initiated reaction (Neutze and Moffat, 2012). A classic example is observation of photodissociation and rebinding of carbon monoxide to myoglobin and hemoglobin (Knapp et al., 2006; Srajer et al., 1996). These time-resolved findings identify myoglobin photoproducts and serve a structural basis to spectroscopic observations and MD calculations. Technical challenges specific for Laue diffraction such as overlap of energies and spots have been effectively dealt with. Maturation of time-resolved X-ray crystallography allowed its application in fragile membrane protein crystals, as evidenced by the direct observation of light-induced changes in a photosynthetic reaction center (Burgess et al., 2003). The emergence of XFELs is transforming the field of time-resolved X-ray crystallography, despite numerous unresolved challenges. In contrast to time-resolved Laue diffraction, which requires crystals, time-resolved wide-angle X-ray scattering (WAXS) allows study of macromolecules in solution and has been successfully applied to a number of proteins, including myoglobin and hemoglobin.

Concluding Remark

X-ray crystallography seemed to be at its pinnacle in the early 1990s, when I, as a motivated graduate student, felt extremely excited by the rapid emergence of crystal structures on biologically important macromolecules. The forecast was that structural biology by X-ray crystallography would become saturated within a few years, leaving structural biologists in an awkward situation of excess in supply. Another prediction, believed by many in the late 1990s, would have structural genomics—automated high-throughput X-ray crystallography—dominate the research landscape. Thankfully, neither prediction was remotely close to fact. X-ray crystallography is alive and well and continues to play an extremely important role in deciphering the secrets of life. In essence, life is all about function and structure, with the former determined by the latter. In the past five decades, structural biology through X-ray crystallography has provided important mechanistic insights into every discipline of modern experimental biology. A large proportion of all display items in the seventh edition of the Jeremy Berg and Lubert Stryer *Biochemistry* textbook are structural images, mostly derived from X-ray crystallographic analyses. X-ray crystallography is at its pinnacle. What follows pinnacle must be a downhill path—would this be true for X-ray crystallography?

In response to a question raised by a motivated, biophysics-oriented student, Doug Rees of Caltech commented at a special seminar at the end of 2013 that "If I were to choose a lab to join for my PhD thesis research, I would probably go for an EM lab." This statement echoes the emotions of those structural biologists who have been so comfortable with X-ray crystallography as the method of choice for elucidating three-dimensional structures of macromolecules. The recent technological advances in cryo-EM, single-particle analysis have sent shockwaves through the entire structural biology community. Near-atomic resolution EM structures have been obtained not only for the megacomplexes such as ribosomes and viruses (Amunts et al., 2014; Zhang et al., 2010) but also for relatively small protein particles exemplified by the TRP channel (Liao et al., 2013). Recently, a 4.5 Å resolution density map was generated for human γ-secretase (Lu et al., 2014), which has a calculated protein molecular weight of only 160 kDa with no symmetry. In the 1990s, the Cold Spring Harbor Laboratory Course on X-ray Crystallography was extremely popular for NMR spectroscopists. That signaled a trend that is still unfolding today. In the 2014 Kuo KH Summer School of Electron Microscopy in Shanghai, a number of established X-ray crystallographers were enrolled as students. There is no doubt that a new trend is in place and will change the pace of structural biology for many years to come.

John Burdon Sanderson Haldane, one of the greatest evolutionary biologists of all times, once declared in his essay, *The Future of Biology*, that "… the future will make any detailed predictions look rather silly." Indeed, the eternal truth in research is that the unexpected always happens. Within the past 2 years, cryo-EM has emerged as a competitive and perhaps even more favored tool for elucidation of macromolecular assemblies with molecular weight of more than 300 kDa. In the foreseeable future, advances in sample preparation and image acquisition will likely expand the advantages of cryo-EM over X-ray crystallography into complexes with smaller molecular weights. On the other hand, technological development of XFEL may strongly affect the comparison of EM versus X-ray. After all, the ultimate goal of XFEL is to make reconstruction of single-molecule scattering possible, namely to visualize single molecules with atomic details in solution. Regardless of these scenarios, X-ray crystallography will continue to dominate structure determination for many years to come, owing to its mature methodology, high resolution, convenient accessibility worldwide, and a vast number of experienced users.

ACKNOWLEDGMENTS

I apologize to those colleagues whose important contributions are not cited in this review due to space limitations. I thank Jiawei Wang, Haipeng Gong, Hongwei Wang, Haitao Li, Frank Yan, Jiawei Wu, and Xinquan Wang for comments and members of my laboratory, particularly Ruobing Ren, Qi Hu, Tian Xie, Dong Deng, Shangyu Dang, Linfeng Sun, and Peilong Lu, for discussion.

REFERENCES

Abate, A.A., Pentimalli, F., Esposito, L., and Giordano, A. (2013). ATP-noncompetitive CDK inhibitors for cancer therapy: an overview. Expert Opin. Investig. Drugs *22*, 895–906.

Abrahams, J.P., Leslie, A.G., Lutter, R., and Walker, J.E. (1994). Structure at 2.8 A resolution of F1-ATPase from bovine heart mitochondria. Nature *370*, 621–628.

Abramson, J., Smirnova, I., Kasho, V., Verner, G., Kaback, H.R., and Iwata, S. (2003). Structure and mechanism of the lactose permease of Escherichia coli. Science *301*, 610–615.

Acharya, R., Fry, E., Stuart, D., Fox, G., Rowlands, D., and Brown, F. (1989). The three-dimensional structure of foot-and-mouth disease virus at 2.9 A resolution. Nature *337*, 709–716.

Adams, P.D., Grosse-Kunstleve, R.W., Hung, L.-W., Ioerger, T.R., McCoy, A.J., Moriarty, N.W., Read, R.J., Sacchettini, J.C., Sauter, N.K., and Terwilliger, T.C. (2002). PHENIX: building new software for automated crystallographic structure determination. Acta Crystallogr. D Biol. Crystallogr. *58*, 1948–1954.

Agah, S., and Faham, S. (2012). Crystallization of membrane proteins in bicelles. Methods Mol. Biol. *914*, 3–16.

Aggarwal, A.K., Rodgers, D.W., Drottar, M., Ptashne, M., and Harrison, S.C. (1988). Recognition of a DNA operator by the repressor of phage 434: a view at high resolution. Science *242*, 899–907.

Alattia, J.R., Matasci, M., Dimitrov, M., Aeschbach, L., Balasubramanian, S., Hacker, D.L., Wurm, F.M., and Fraering, P.C. (2013). Highly efficient production of the Alzheimer's γ-secretase integral membrane protease complex by a multi-gene stable integration approach. Biotechnol. Bioeng. *110*, 1995–2005.

Allen, J.P., Feher, G., Yeates, T.O., Komiya, H., and Rees, D.C. (1987). Structure of the reaction center from Rhodobacter sphaeroides R-26: the protein subunits. Proc. Natl. Acad. Sci. USA *84*, 6162–6166.

Amunts, A., Brown, A., Bai, X.C., Llácer, J.L., Hussain, T., Emsley, P., Long, F., Murshudov, G., Scheres, S.H., and Ramakrishnan, V. (2014). Structure of the yeast mitochondrial large ribosomal subunit. Science *343*, 1485–1489.

Anderson, J.E., Ptashne, M., and Harrison, S.C. (1987). Structure of the repressor-operator complex of bacteriophage 434. Nature *326*, 846–852.

Arndt, U.W., and Wonacott, A. (1977). Rotation method in crystallography (North-Holland: Amsterdam).

Assenberg, R., Wan, P.T., Geisse, S., and Mayr, L.M. (2013). Advances in recombinant protein expression for use in pharmaceutical research. Curr. Opin. Struct. Biol. *23*, 393–402.

Baase, W.A., Liu, L., Tronrud, D.E., and Matthews, B.W. (2010). Lessons from the lysozyme of phage T4. Protein Sci. *19*, 631–641.

Ban, N., Nissen, P., Hansen, J., Moore, P.B., and Steitz, T.A. (2000). The complete atomic structure of the large ribosomal subunit at 2.4 A resolution. Science *289*, 905–920.

Banner, D.W., D'Arcy, A., Janes, W., Gentz, R., Schoenfeld, H.J., Broger, C., Loetscher, H., and Lesslauer, W. (1993). Crystal structure of the soluble human 55 kd TNF receptor-human TNF beta complex: implications for TNF receptor activation. Cell *73*, 431–445.

Barends, T.R., Foucar, L., Botha, S., Doak, R.B., Shoeman, R.L., Nass, K., Koglin, J.E., Williams, G.J., Boutet, S., Messerschmidt, M., and Schlichting, I. (2014). De novo protein crystal structure determination from X-ray free-electron laser data. Nature *505*, 244–247.

Bass, R.B., Strop, P., Barclay, M., and Rees, D.C. (2002). Crystal structure of Escherichia coli MscS, a voltage-modulated and mechanosensitive channel. Science *298*, 1582–1587.

Beck, F., Unverdorben, P., Bohn, S., Schweitzer, A., Pfeifer, G., Sakata, E., Nickell, S., Plitzko, J.M., Villa, E., Baumeister, W., and Förster, F. (2012). Near-atomic resolution structural model of the yeast 26S proteasome. Proc. Natl. Acad. Sci. USA *109*, 14870–14875.

Ben-Shem, A., Fass, D., and Bibi, E. (2007). Structural basis for intramembrane proteolysis by rhomboid serine proteases. Proc. Natl. Acad. Sci. USA *104*, 462–466.

Blake, C.C., Koenig, D.F., Mair, G.A., North, A.C., Phillips, D.C., and Sarma, V.R. (1965). Structure of hen egg-white lysozyme. A three-dimensional Fourier synthesis at 2 Angstrom resolution. Nature *206*, 757–761.

Bloomer, A.C., Champness, J.N., Bricogne, G., Staden, R., and Klug, A. (1978). Protein disk of tobacco mosaic virus at 2.8 A resolution showing the interactions within and between subunits. Nature *276*, 362–368.

Boggon, T.J., and Shapiro, L. (2000). Screening for phasing atoms in protein crystallography. Structure *8*, R143–R149.

Bonneau, F., Basquin, J., Ebert, J., Lorentzen, E., and Conti, E. (2009). The yeast exosome functions as a macromolecular cage to channel RNA substrates for degradation. Cell *139*, 547–559.

Bostick, D.L., and Brooks, C.L., 3rd. (2007). Selectivity in K+ channels is due to topological control of the permeant ion's coordinated state. Proc. Natl. Acad. Sci. USA *104*, 9260–9265.

Boutet, S., Lomb, L., Williams, G.J., Barends, T.R., Aquila, A., Doak, R.B., Weierstall, U., DePonte, D.P., Steinbrener, J., Shoeman, R.L., et al. (2012). High-resolution protein structure determination by serial femtosecond crystallography. Science *337*, 362–364.

Bragg, W.L. (1913). The diffraction of short electromagnetic waves by a crystal. Proceedings of the Cambridge Philosophical Society *17*, 43–57.

Brotherton, D.H., Dhanaraj, V., Wick, S., Brizuela, L., Domaille, P.J., Volyanik, E., Xu, X., Parisini, E., Smith, B.O., Archer, S.J., et al. (1998). Crystal structure of the complex of the cyclin D-dependent kinase Cdk6 bound to the cell-cycle inhibitor p19INK4d. Nature *395*, 244–250.

Brown, M.S., Ye, J., Rawson, R.B., and Goldstein, J.L. (2000). Regulated intramembrane proteolysis: a control mechanism conserved from bacteria to humans. Cell *100*, 391–398.

Brunger, A. (1990). XPLOR Manual, v 2.1 (New Haven: Yale University).

Brünger, A.T. (1992). Free R value: a novel statistical quantity for assessing the accuracy of crystal structures. Nature *355*, 472–475.

Brünger, A.T., Adams, P.D., Clore, G.M., DeLano, W.L., Gros, P., Grosse-Kunstleve, R.W., Jiang, J.-S., Kuszewski, J., Nilges, M., Pannu, N.S., et al. (1998). Crystallography & NMR system: A new software suite for macromolecular structure determination. Acta Crystallogr. D Biol. Crystallogr. *54*, 905–921.

Burgess, A.W., Cho, H.S., Eigenbrot, C., Ferguson, K.M., Garrett, T.P., Leahy, D.J., Lemmon, M.A., Sliwkowski, M.X., Ward, C.W., and Yokoyama, S. (2003). An open-and-shut case? Recent insights into the activation of EGF/ErbB receptors. Mol. Cell *12*, 541–552.

Caffrey, M. (2009). Crystallizing membrane proteins for structure determination: use of lipidic mesophases. Annu. Rev. Biophys. *38*, 29–51.

Chang, G., Spencer, R.H., Lee, A.T., Barclay, M.T., and Rees, D.C. (1998). Structure of the MscL homolog from Mycobacterium tuberculosis: a gated mechanosensitive ion channel. Science *282*, 2220–2226.

Chapman, H.N., Fromme, P., Barty, A., White, T.A., Kirian, R.A., Aquila, A., Hunter, M.S., Schulz, J., DePonte, D.P., Weierstall, U., et al. (2011). Femtosecond X-ray protein nanocrystallography. Nature *470*, 73–77.

Chen, S., Oldham, M.L., Davidson, A.L., and Chen, J. (2013). Carbon catabolite repression of the maltose transporter revealed by X-ray crystallography. Nature *499*, 364–368.

Chen, L., Duerr, K.L., and Gouaux, E. (2014). X-ray structures of AMPA receptor-cone snail toxin complexes illuminate activation mechanism. Science *345*, 1021–1026.

Cherezov, V., Rosenbaum, D.M., Hanson, M.A., Rasmussen, S.G., Thian, F.S., Kobilka, T.S., Choi, H.J., Kuhn, P., Weis, W.I., Kobilka, B.K., and Stevens, R.C. (2007). High-resolution crystal structure of an engineered human beta2-adrenergic G protein-coupled receptor. Science *318*, 1258–1265.

Cherezov, V., Abola, E., and Stevens, R.C. (2010). Recent progress in the structure determination of GPCRs, a membrane protein family with high potential as pharmaceutical targets. Methods Mol. Biol. *654*, 141–168.

Cho, H.S., Mason, K., Ramyar, K.X., Stanley, A.M., Gabelli, S.B., Denney, D.W., Jr., and Leahy, D.J. (2003). Structure of the extracellular region of HER2 alone and in complex with the Herceptin Fab. Nature *421*, 756–760.

Collaborative, C.P.; Collaborative Computational Project, Number 4 (1994). The CCP4 suite: programs for protein crystallography. Acta Crystallogr. D Biol. Crystallogr. *50*, 760–763.

Cramer, P. (2014). A tale of chromatin and transcription in 100 structures. Cell *159*, this issue, 985–994.

Dang, S., Sun, L., Huang, Y., Lu, F., Liu, Y., Gong, H., Wang, J., and Yan, N. (2010). Structure of a fucose transporter in an outward-open conformation. Nature *467*, 734–738.

Dauter, Z. (2005). Use of polynuclear metal clusters in protein crystallography. C. R. Chim. *8*, 1808–1814.

Dawson, R.J., and Locher, K.P. (2006). Structure of a bacterial multidrug ABC transporter. Nature *443*, 180–185.

De Bondt, H.L., Rosenblatt, J., Jancarik, J., Jones, H.D., Morgan, D.O., and Kim, S.H. (1993). Crystal structure of cyclin-dependent kinase 2. Nature *363*, 595–602.

de Vos, A.M., Ultsch, M., and Kossiakoff, A.A. (1992). Human growth hormone and extracellular domain of its receptor: crystal structure of the complex. Science *255*, 306–312.

Deisenhofer, J., Epp, O., Miki, K., Huber, R., and Michel, H. (1985). Structure of the protein subunits in the photosynthetic reaction centre of Rhodopseudomonas viridis at 3Å resolution. Nature *318*, 618–624.

Deng, D., Xu, C., Sun, P., Wu, J., Yan, C., Hu, M., and Yan, N. (2014). Crystal structure of the human glucose transporter GLUT1. Nature *510*, 121–125.

Doyle, D.A., Lee, A., Lewis, J., Kim, E., Sheng, M., and MacKinnon, R. (1996). Crystal structures of a complexed and peptide-free membrane protein-binding domain: molecular basis of peptide recognition by PDZ. Cell *85*, 1067–1076.

Doyle, D.A., Morais Cabral, J., Pfuetzner, R.A., Kuo, A., Gulbis, J.M., Cohen, S.L., Chait, B.T., and MacKinnon, R. (1998). The structure of the potassium channel: molecular basis of K+ conduction and selectivity. Science *280*, 69–77.

Drenth, J., Jansonius, J.N., Koekoek, R., Swen, H.M., and Wolthers, B.G. (1968). Structure of papain. Nature *218*, 929–932.

Dürr, K.L., Chen, L., Stein, R.A., De Zorzi, R., Folea, I.M., Walz, T., Mchaourab, H.S., and Gouaux, E. (2014). Structure and dynamics of AMPA receptor GluA2 in resting, pre-open, and desensitized states. Cell *158*, 778–792.

Emsley, P., and Cowtan, K. (2004). Coot: model-building tools for molecular graphics. Acta Crystallogr. D Biol. Crystallogr. *60*, 2126–2132.

Faham, S., Watanabe, A., Besserer, G.M., Cascio, D., Specht, A., Hirayama, B.A., Wright, E.M., and Abramson, J. (2008). The crystal structure of a sodium galactose transporter reveals mechanistic insights into Na+/sugar symport. Science *321*, 810–814.

Fang, Y., Jayaram, H., Shane, T., Kolmakova-Partensky, L., Wu, F., Williams, C., Xiong, Y., and Miller, C. (2009). Structure of a prokaryotic virtual proton pump at 3.2 A resolution. Nature *460*, 1040–1043.

Feng, L., Yan, H., Wu, Z., Yan, N., Wang, Z., Jeffrey, P.D., and Shi, Y. (2007). Structure of a site-2 protease family intramembrane metalloprotease. Science *318*, 1608–1612.

Ferguson, K.M., Lemmon, M.A., Schlessinger, J., and Sigler, P.B. (1995). Structure of the high affinity complex of inositol trisphosphate with a phospholipase C pleckstrin homology domain. Cell *83*, 1037–1046.

Finch, J.T., Lutter, L.C., Rhodes, D., Brown, R.S., Rushton, B., Levitt, M., and Klug, A. (1977). Structure of nucleosome core particles of chromatin. Nature *269*, 29–36.

Fischer, E.H., and Krebs, E.G. (1955). Conversion of phosphorylase b to phosphorylase a in muscle extracts. J. Biol. Chem. *216*, 121–132.

Franklin, M.C., Carey, K.D., Vajdos, F.F., Leahy, D.J., de Vos, A.M., and Sliwkowski, M.X. (2004). Insights into ErbB signaling from the structure of the ErbB2-pertuzumab complex. Cancer Cell *5*, 317–328.

Fu, D., Libson, A., Miercke, L.J., Weitzman, C., Nollert, P., Krucinski, J., and Stroud, R.M. (2000). Structure of a glycerol-conducting channel and the basis for its selectivity. Science *290*, 481–486.

Gao, X., Lu, F., Zhou, L., Dang, S., Sun, L., Li, X., Wang, J., and Shi, Y. (2009). Structure and mechanism of an amino acid antiporter. Science *324*, 1565–1568.

Gao, X., Zhou, L., Jiao, X., Lu, F., Yan, C., Zeng, X., Wang, J., and Shi, Y. (2010). Mechanism of substrate recognition and transport by an amino acid antiporter. Nature *463*, 828–832.

Garboczi, D.N., Ghosh, P., Utz, U., Fan, Q.R., Biddison, W.E., and Wiley, D.C. (1996). Structure of the complex between human T-cell receptor, viral peptide and HLA-A2. Nature *384*, 134–141.

Garcia, K.C., Degano, M., Stanfield, R.L., Brunmark, A., Jackson, M.R., Peterson, P.A., Teyton, L., and Wilson, I.A. (1996). An alphabeta T cell receptor structure at 2.5 A and its orientation in the TCR-MHC complex. Science *274*, 209–219.

Garrett, T.P., McKern, N.M., Lou, M., Elleman, T.C., Adams, T.E., Lovrecz, G.O., Zhu, H.J., Walker, F., Frenkel, M.J., Hoyne, P.A., et al. (2002). Crystal structure of a truncated epidermal growth factor receptor extracellular domain bound to transforming growth factor alpha. Cell *110*, 763–773.

Gerber, S., Comellas-Bigler, M., Goetz, B.A., and Locher, K.P. (2008). Structural basis of trans-inhibition in a molybdate/tungstate ABC transporter. Science *321*, 246–250.

Gonen, T., Cheng, Y., Sliz, P., Hiroaki, Y., Fujiyoshi, Y., Harrison, S.C., and Walz, T. (2005). Lipid-protein interactions in double-layered two-dimensional AQP0 crystals. Nature *438*, 633–638.

Grigorieff, N., Ceska, T.A., Downing, K.H., Baldwin, J.M., and Henderson, R. (1996). Electron-crystallographic refinement of the structure of bacteriorhodopsin. J. Mol. Biol. *259*, 393–421.

Groll, M., Ditzel, L., Löwe, J., Stock, D., Bochtler, M., Bartunik, H.D., and Huber, R. (1997). Structure of 20S proteasome from yeast at 2.4 A resolution. Nature *386*, 463–471.

Harrison, S.C. (1969). Structure of tomato bushy stunt virus. I. The spherically averaged electron density. J. Mol. Biol. *42*, 457–483.

Harrison, S.C., and Jack, A. (1975). Structure of tomato bushy stunt virus. Three-dimensional x-ray diffraction analysis at 16 A resolution. J. Mol. Biol. *97*, 173–191.

Harrison, S.C., Olson, A.J., Schutt, C.E., Winkler, F.K., and Bricogne, G. (1978). Tomato bushy stunt virus at 2.9 A resolution. Nature *276*, 368–373.

Hattne, J., Echols, N., Tran, R., Kern, J., Gildea, R.J., Brewster, A.S., Alonso-Mori, R., Glöckner, C., Hellmich, J., Laksmono, H., et al. (2014). Accurate macromolecular structures using minimal measurements from X-ray free-electron lasers. Nat. Methods *11*, 545–548.

Huang, Y., Lemieux, M.J., Song, J., Auer, M., and Wang, D.N. (2003). Structure and mechanism of the glycerol-3-phosphate transporter from Escherichia coli. Science *301*, 616–620.

Hvorup, R.N., Goetz, B.A., Niederer, M., Hollenstein, K., Perozo, E., and Locher, K.P. (2007). Asymmetry in the structure of the ABC transporter-binding protein complex BtuCD-BtuF. Science *317*, 1387–1390.

Jardetzky, O. (1966). Simple allosteric model for membrane pumps. Nature *211*, 969–970.

Jeffrey, P.D., Russo, A.A., Polyak, K., Gibbs, E., Hurwitz, J., Massagué, J., and Pavletich, N.P. (1995). Mechanism of CDK activation revealed by the structure of a cyclinA-CDK2 complex. Nature *376*, 313–320.

Jiang, Y., Lee, A., Chen, J., Cadene, M., Chait, B.T., and MacKinnon, R. (2002). Crystal structure and mechanism of a calcium-gated potassium channel. Nature *417*, 515–522.

Jiang, Y., Ruta, V., Chen, J., Lee, A., and MacKinnon, R. (2003). The principle of gating charge movement in a voltage-dependent K+ channel. Nature *423*, 42–48.

Joachimiak, A. (2009). High-throughput crystallography for structural genomics. Curr. Opin. Struct. Biol. *19*, 573–584.

Jones, T.A., Zou, J.-Y., Cowan, S.W., and Kjeldgaard, M. (1991). Improved methods for building protein models in electron density maps and the location of errors in these models. Acta Crystallogr. A *47*, 110–119.

Kaback, H.R. (2005). Structure and mechanism of the lactose permease. C. R. Biol. *328*, 557–567.

Kadaba, N.S., Kaiser, J.T., Johnson, E., Lee, A., and Rees, D.C. (2008). The high-affinity E. coli methionine ABC transporter: structure and allosteric regulation. Science *321*, 250–253.

Karakas, E., and Furukawa, H. (2014). Crystal structure of a heterotetrameric NMDA receptor ion channel. Science *344*, 992–997.

Kartha, G., Bello, J., and Harker, D. (1967). Tertiary structure of ribonuclease. Nature *213*, 862–865.

Kendrew, J.C., Bodo, G., Dintzis, H.M., Parrish, R.G., Wyckoff, H., and Phillips, D.C. (1958). A three-dimensional model of the myoglobin molecule obtained by x-ray analysis. Nature *181*, 662–666.

Kendrew, J.C., Dickerson, R.E., Strandberg, B.E., Hart, R.G., Davies, D.R., Phillips, D.C., and Shore, V.C. (1960). Structure of myoglobin: A three-dimensional Fourier synthesis at 2 A. resolution. Nature *185*, 422–427.

Kern, J., Alonso-Mori, R., Tran, R., Hattne, J., Gildea, R.J., Echols, N., Glöckner, C., Hellmich, J., Laksmono, H., Sierra, R.G., et al. (2013). Simultaneous

femtosecond X-ray spectroscopy and diffraction of photosystem II at room temperature. Science *340*, 491–495.

Khare, D., Oldham, M.L., Orelle, C., Davidson, A.L., and Chen, J. (2009). Alternating access in maltose transporter mediated by rigid-body rotations. Mol. Cell *33*, 528–536.

Kim, C., Xuong, N.H., and Taylor, S.S. (2005). Crystal structure of a complex between the catalytic and regulatory (RIalpha) subunits of PKA. Science *307*, 690–696.

Knapp, J.E., Pahl, R., Srajer, V., and Royer, W.E., Jr. (2006). Allosteric action in real time: time-resolved crystallographic studies of a cooperative dimeric hemoglobin. Proc. Natl. Acad. Sci. USA *103*, 7649–7654.

Knighton, D.R., Zheng, J.H., Ten Eyck, L.F., Ashford, V.A., Xuong, N.H., Taylor, S.S., and Sowadski, J.M. (1991). Crystal structure of the catalytic subunit of cyclic adenosine monophosphate-dependent protein kinase. Science *253*, 407–414.

Kobilka, B.K., Dixon, R.A., Frielle, T., Dohlman, H.G., Bolanowski, M.A., Sigal, I.S., Yang-Feng, T.L., Francke, U., Caron, M.G., and Lefkowitz, R.J. (1987a). cDNA for the human beta 2-adrenergic receptor: a protein with multiple membrane-spanning domains and encoded by a gene whose chromosomal location is shared with that of the receptor for platelet-derived growth factor. Proc. Natl. Acad. Sci. USA *84*, 46–50.

Kobilka, B.K., Matsui, H., Kobilka, T.S., Yang-Feng, T.L., Francke, U., Caron, M.G., Lefkowitz, R.J., and Regan, J.W. (1987b). Cloning, sequencing, and expression of the gene coding for the human platelet alpha 2-adrenergic receptor. Science *238*, 650–656.

Kobilka, B.K., Kobilka, T.S., Daniel, K., Regan, J.W., Caron, M.G., and Lefkowitz, R.J. (1988). Chimeric alpha 2-,beta 2-adrenergic receptors: delineation of domains involved in effector coupling and ligand binding specificity. Science *240*, 1310–1316.

Kraft, P., Bergamaschi, A., Broennimann, Ch., Dinapoli, R., Eikenberry, E.F., Henrich, B., Johnson, I., Mozzanica, A., Schlepütz, C.M., Willmott, P.R., and Schmitt, B. (2009). Performance of single-photon-counting PILATUS detector modules. J. Synchrotron Radiat. *16*, 368–375.

Kühlbrandt, W., Wang, D.N., and Fujiyoshi, Y. (1994). Atomic model of plant light-harvesting complex by electron crystallography. Nature *367*, 614–621.

Lee, C.H., Lü, W., Michel, J.C., Goehring, A., Du, J., Song, X., and Gouaux, E. (2014). NMDA receptor structures reveal subunit arrangement and pore architecture. Nature *511*, 191–197.

Lemieux, M.J., Fischer, S.J., Cherney, M.M., Bateman, K.S., and James, M.N. (2007). The crystal structure of the rhomboid peptidase from Haemophilus influenzae provides insight into intramembrane proteolysis. Proc. Natl. Acad. Sci. USA *104*, 750–754.

Leung, A.K., Nagai, K., and Li, J. (2011). Structure of the spliceosomal U4 snRNP core domain and its implication for snRNP biogenesis. Nature *473*, 536–539.

Li, S., Schmitz, K.R., Jeffrey, P.D., Wiltzius, J.J., Kussie, P., and Ferguson, K.M. (2005). Structural basis for inhibition of the epidermal growth factor receptor by cetuximab. Cancer Cell *7*, 301–311.

Li, X., Dang, S., Yan, C., Gong, X., Wang, J., and Shi, Y. (2013). Structure of a presenilin family intramembrane aspartate protease. Nature *493*, 56–61.

Liao, M., Cao, E., Julius, D., and Cheng, Y. (2013). Structure of the TRPV1 ion channel determined by electron cryo-microscopy. Nature *504*, 107–112.

Lindorff-Larsen, K., Piana, S., Dror, R.O., and Shaw, D.E. (2011). How fast-folding proteins fold. Science *334*, 517–520.

Lingaraju, G.M., Bunker, R.D., Cavadini, S., Hess, D., Hassiepen, U., Renatus, M., Fischer, E.S., and Thomä, N.H. (2014). Crystal structure of the human COP9 signalosome. Nature *512*, 161–165.

Lipscomb, W.N., Hartsuck, J.A., Quiocho, F.A., and Reeke, G.N., Jr. (1969). The structure of carboxypeptidase A. IX. The x-ray diffraction results in the light of the chemical sequence. Proc. Natl. Acad. Sci. USA *64*, 28–35.

Liu, Q., Greimann, J.C., and Lima, C.D. (2006). Reconstitution, activities, and structure of the eukaryotic RNA exosome. Cell *127*, 1223–1237.

Liu, W., Wacker, D., Gati, C., Han, G.W., James, D., Wang, D., Nelson, G., Weierstall, U., Katritch, V., Barty, A., et al. (2013). Serial femtosecond crystallography of G protein-coupled receptors. Science *342*, 1521–1524.

Locher, K.P., Lee, A.T., and Rees, D.C. (2002). The E. coli BtuCD structure: a framework for ABC transporter architecture and mechanism. Science *296*, 1091–1098.

Long, S.B., Campbell, E.B., and Mackinnon, R. (2005). Crystal structure of a mammalian voltage-dependent Shaker family K+ channel. Science *309*, 897–903.

Löwe, J., Stock, D., Jap, B., Zwickl, P., Baumeister, W., and Huber, R. (1995). Crystal structure of the 20S proteasome from the archaeon T. acidophilum at 3.4 A resolution. Science *268*, 533–539.

Lu, P., Bai, X.C., Ma, D., Xie, T., Yan, C., Sun, L., Yang, G., Zhao, Y., Zhou, R., Scheres, S.H., and Shi, Y. (2014). Three-dimensional structure of human γ-secretase. Nature *512*, 166–170.

Luger, K., Mäder, A.W., Richmond, R.K., Sargent, D.F., and Richmond, T.J. (1997). Crystal structure of the nucleosome core particle at 2.8 A resolution. Nature *389*, 251–260.

Luo, M., Vriend, G., Kamer, G., Minor, I., Arnold, E., Rossmann, M.G., Boege, U., Scraba, D.G., Duke, G.M., and Palmenberg, A.C. (1987). The atomic structure of Mengo virus at 3.0 A resolution. Science *235*, 182–191.

Lynch, T.J., Bell, D.W., Sordella, R., Gurubhagavatula, S., Okimoto, R.A., Brannigan, B.W., Harris, P.L., Haserlat, S.M., Supko, J.G., Haluska, F.G., et al. (2004). Activating mutations in the epidermal growth factor receptor underlying responsiveness of non-small-cell lung cancer to gefitinib. N. Engl. J. Med. *350*, 2129–2139.

Ma, D., Lu, P., Yan, C., Fan, C., Yin, P., Wang, J., and Shi, Y. (2012). Structure and mechanism of a glutamate-GABA antiporter. Nature *483*, 632–636.

MacKinnon, R. (2003). Potassium channels. FEBS Lett. *555*, 62–65.

Makino, D.L., Baumgärtner, M., and Conti, E. (2013). Crystal structure of an RNA-bound 11-subunit eukaryotic exosome complex. Nature *495*, 70–75.

Matthews, B.W., and Remington, S.J. (1974). The three dimensional structure of the lysozyme from bacteriophage T4. Proc. Natl. Acad. Sci. USA *71*, 4178–4182.

Matthews, B.W., Sigler, P.B., Henderson, R., and Blow, D.M. (1967). Three-dimensional structure of tosyl-alpha-chymotrypsin. Nature *214*, 652–656.

McPherson, A., and Gavira, J.A. (2014). Introduction to protein crystallization. Acta Crystallogr. F Struct. Biol. Commun. *70*, 2–20.

Montemayor, E.J., Curran, E.C., Liao, H.H., Andrews, K.L., Treba, C.N., Butcher, S.E., and Brow, D.A. (2014). Core structure of the U6 small nuclear ribonucleoprotein at 1.7-Å resolution. Nat. Struct. Mol. Biol. *21*, 544–551.

Morais-Cabral, J.H., Zhou, Y., and MacKinnon, R. (2001). Energetic optimization of ion conduction rate by the K+ selectivity filter. Nature *414*, 37–42.

Morth, J.P., Sørensen, T.L., and Nissen, P. (2006). Membrane's Eleven: heavy-atom derivatives of membrane-protein crystals. Acta Crystallogr. D Biol. Crystallogr. *62*, 877–882.

Musacchio, A., Noble, M., Pauptit, R., Wierenga, R., and Saraste, M. (1992). Crystal structure of a Src-homology 3 (SH3) domain. Nature *359*, 851–855.

Musacchio, A., Saraste, M., and Wilmanns, M. (1994). High-resolution crystal structures of tyrosine kinase SH3 domains complexed with proline-rich peptides. Nat. Struct. Biol. *1*, 546–551.

Nagar, B., Bornmann, W.G., Pellicena, P., Schindler, T., Veach, D.R., Miller, W.T., Clarkson, B., and Kuriyan, J. (2002). Crystal structures of the kinase domain of c-Abl in complex with the small molecule inhibitors PD173955 and imatinib (STI-571). Cancer Res. *62*, 4236–4243.

Neutze, R., and Moffat, K. (2012). Time-resolved structural studies at synchrotrons and X-ray free electron lasers: opportunities and challenges. Curr. Opin. Struct. Biol. *22*, 651–659.

Neutze, R., Wouts, R., van der Spoel, D., Weckert, E., and Hajdu, J. (2000). Potential for biomolecular imaging with femtosecond X-ray pulses. Nature *406*, 752–757.

Newstead, S., Drew, D., Cameron, A.D., Postis, V.L., Xia, X., Fowler, P.W., Ingram, J.C., Carpenter, E.P., Sansom, M.S., McPherson, M.J., et al. (2011). Crystal structure of a prokaryotic homologue of the mammalian oligopeptide-proton symporters, PepT1 and PepT2. EMBO J. *30*, 417–426.

Noskov, S.Y., Bernèche, S., and Roux, B. (2004). Control of ion selectivity in potassium channels by electrostatic and dynamic properties of carbonyl ligands. Nature *431*, 830–834.

Ogiso, H., Ishitani, R., Nureki, O., Fukai, S., Yamanaka, M., Kim, J.H., Saito, K., Sakamoto, A., Inoue, M., Shirouzu, M., and Yokoyama, S. (2002). Crystal structure of the complex of human epidermal growth factor and receptor extracellular domains. Cell *110*, 775–787.

Oldham, M.L., and Chen, J. (2011a). Crystal structure of the maltose transporter in a pretranslocation intermediate state. Science *332*, 1202–1205.

Oldham, M.L., and Chen, J. (2011b). Snapshots of the maltose transporter during ATP hydrolysis. Proc. Natl. Acad. Sci. USA *108*, 15152–15156.

Oldham, M.L., Khare, D., Quiocho, F.A., Davidson, A.L., and Chen, J. (2007). Crystal structure of a catalytic intermediate of the maltose transporter. Nature *450*, 515–521.

Olesen, C., Sørensen, T.L., Nielsen, R.C., Møller, J.V., and Nissen, P. (2004). Dephosphorylation of the calcium pump coupled to counterion occlusion. Science *306*, 2251–2255.

Olesen, C., Picard, M., Winther, A.M., Gyrup, C., Morth, J.P., Oxvig, C., Møller, J.V., and Nissen, P. (2007). The structural basis of calcium transport by the calcium pump. Nature *450*, 1036–1042.

Otwinowski, Z., Schevitz, R.W., Zhang, R.G., Lawson, C.L., Joachimiak, A., Marmorstein, R.Q., Luisi, B.F., and Sigler, P.B. (1988). Crystal structure of trp repressor/operator complex at atomic resolution. Nature *335*, 321–329.

Paez, J.G., Jänne, P.A., Lee, J.C., Tracy, S., Greulich, H., Gabriel, S., Herman, P., Kaye, F.J., Lindeman, N., Boggon, T.J., et al. (2004). EGFR mutations in lung cancer: correlation with clinical response to gefitinib therapy. Science *304*, 1497–1500.

Palczewski, K., Kumasaka, T., Hori, T., Behnke, C.A., Motoshima, H., Fox, B.A., Le Trong, I., Teller, D.C., Okada, T., Stenkamp, R.E., et al. (2000). Crystal structure of rhodopsin: A G protein-coupled receptor. Science *289*, 739–745.

Pannu, N.S., and Read, R.J. (1996). Improved structure refinement through maximum likelihood. Acta Crystallogr. A *52*, 659–668.

Pauling, L., and Corey, R.B. (1951a). Atomic coordinates and structure factors for two helical configurations of polypeptide chains. Proc. Natl. Acad. Sci. USA *37*, 235–240.

Pauling, L., and Corey, R.B. (1951b). Configuration of polypeptide chains. Nature *168*, 550–551.

Pauling, L., and Corey, R.B. (1951c). The polypeptide-chain configuration in hemoglobin and other globular proteins. Proc. Natl. Acad. Sci. USA *37*, 282–285.

Pauling, L., Corey, R.B., and Branson, H.R. (1951). The structure of proteins; two hydrogen-bonded helical configurations of the polypeptide chain. Proc. Natl. Acad. Sci. USA *37*, 205–211.

Pavletich, N.P., Chambers, K.A., and Pabo, C.O. (1993). The DNA-binding domain of p53 contains the four conserved regions and the major mutation hot spots. Genes Dev. *7*(12B), 2556–2564.

Pebay-Peyroula, E., Rummel, G., Rosenbusch, J.P., and Landau, E.M. (1997). X-ray structure of bacteriorhodopsin at 2.5 angstroms from microcrystals grown in lipidic cubic phases. Science *277*, 1676–1681.

Perutz, M.F., Rossmann, M.G., Cullis, A.F., Muirhead, H., Will, G., and North, A.C. (1960). Structure of haemoglobin: a three-dimensional Fourier synthesis at 5.5-A. resolution, obtained by X-ray analysis. Nature *185*, 416–422.

Perutz, M.F., Miurhead, H., Cox, J.M., Goaman, L.C., Mathews, F.S., McGandy, E.L., and Webb, L.E. (1968a). Three-dimensional Fourier synthesis of horse oxyhaemoglobin at 2.8 A resolution: (1) x-ray analysis. Nature *219*, 29–32.

Perutz, M.F., Muirhead, H., Cox, J.M., and Goaman, L.C. (1968b). Three-dimensional Fourier synthesis of horse oxyhaemoglobin at 2.8 A resolution: the atomic model. Nature *219*, 131–139.

Phillips, J.C., and Hodgson, K.O. (1980). The use of anomalous scattering effects to phase diffraction patterns from macromolecules. Acta Crystallogr. A *36*, 856–864.

Phillips, W.C., Li, Y., Stanton, M., Xie, J., O'Mara, D., and Kalata, K. (1993). A CCD-based area detector for X-ray crystallography using synchrotron and laboratory sources. Nucl. Instrum. Methods Phys. Res. A *334*, 621–630.

Pinkett, H.W., Lee, A.T., Lum, P., Locher, K.P., and Rees, D.C. (2007). An inward-facing conformation of a putative metal-chelate-type ABC transporter. Science *315*, 373–377.

Pomeranz Krummel, D.A., Oubridge, C., Leung, A.K., Li, J., and Nagai, K. (2009). Crystal structure of human spliceosomal U1 snRNP at 5.5 A resolution. Nature *458*, 475–480.

Rasmussen, S.G., Choi, H.J., Rosenbaum, D.M., Kobilka, T.S., Thian, F.S., Edwards, P.C., Burghammer, M., Ratnala, V.R., Sanishvili, R., Fischetti, R.F., et al. (2007). Crystal structure of the human beta2 adrenergic G-protein-coupled receptor. Nature *450*, 383–387.

Rasmussen, S.G., DeVree, B.T., Zou, Y., Kruse, A.C., Chung, K.Y., Kobilka, T.S., Thian, F.S., Chae, P.S., Pardon, E., Calinski, D., et al. (2011). Crystal structure of the β2 adrenergic receptor-Gs protein complex. Nature *477*, 549–555.

Recondo, G., Dìaz Canton, E., de la Vega, M., Greco, M., Recondo, G., and Valsecchi, M.E. (2014). Therapeutic options for HER-2 positive breast cancer: Perspectives and future directions. World J. Clin. Oncol. *5*, 440–454.

Redecke, L., Nass, K., DePonte, D.P., White, T.A., Rehders, D., Barty, A., Stellato, F., Liang, M., Barends, T.R., Boutet, S., et al. (2013). Natively inhibited Trypanosoma brucei cathepsin B structure determined by using an X-ray laser. Science *339*, 227–230.

Ressl, S., Terwisscha van Scheltinga, A.C., Vonrhein, C., Ott, V., and Ziegler, C. (2009). Molecular basis of transport and regulation in the Na(+)/betaine symporter BetP. Nature *458*, 47–52.

Richmond, T.J., Finch, J.T., Rushton, B., Rhodes, D., and Klug, A. (1984). Structure of the nucleosome core particle at 7 A resolution. Nature *311*, 532–537.

Rodgers, D.W. (1994). Cryocrystallography. Structure *2*, 1135–1140.

Rosenbaum, G., and Holmes, K. (1971). Synchrotron radiation as a source for X-ray diffraction. Nature *230*, 434–437.

Rosenbaum, D.M., Cherezov, V., Hanson, M.A., Rasmussen, S.G., Thian, F.S., Kobilka, T.S., Choi, H.J., Yao, X.J., Weis, W.I., Stevens, R.C., and Kobilka, B.K. (2007). GPCR engineering yields high-resolution structural insights into beta2-adrenergic receptor function. Science *318*, 1266–1273.

Rossmann, M.G., Arnold, E., Erickson, J.W., Frankenberger, E.A., Griffith, J.P., Hecht, H.J., Johnson, J.E., Kamer, G., Luo, M., Mosser, A.G., et al. (1985). Structure of a human common cold virus and functional relationship to other picornaviruses. Nature *317*, 145–153.

Roux, B., and MacKinnon, R. (1999). The cavity and pore helices in the KcsA K+ channel: electrostatic stabilization of monovalent cations. Science *285*, 100–102.

Russo, A.A., Jeffrey, P.D., Patten, A.K., Massagué, J., and Pavletich, N.P. (1996a). Crystal structure of the p27Kip1 cyclin-dependent-kinase inhibitor bound to the cyclin A-Cdk2 complex. Nature *382*, 325–331.

Russo, A.A., Jeffrey, P.D., and Pavletich, N.P. (1996b). Structural basis of cyclin-dependent kinase activation by phosphorylation. Nat. Struct. Biol. *3*, 696–700.

Russo, A.A., Tong, L., Lee, J.O., Jeffrey, P.D., and Pavletich, N.P. (1998). Structural basis for inhibition of the cyclin-dependent kinase Cdk6 by the tumour suppressor p16INK4a. Nature *395*, 237–243.

Saier, M.H., Jr., Yen, M.R., Noto, K., Tamang, D.G., and Elkan, C. (2009). The Transporter Classification Database: recent advances. Nucleic Acids Res. *37*, D274–D278.

Savage, D.F., Egea, P.F., Robles-Colmenares, Y., O'Connell, J.D., 3rd, and Stroud, R.M. (2003). Architecture and selectivity in aquaporins: 2.5 a X-ray structure of aquaporin Z. PLoS Biol. *1*, E72.

Schindler, T., Bornmann, W., Pellicena, P., Miller, W.T., Clarkson, B., and Kuriyan, J. (2000). Structural mechanism for STI-571 inhibition of abelson tyrosine kinase. Science *289*, 1938–1942.

Seemüller, E., Lupas, A., Stock, D., Löwe, J., Huber, R., and Baumeister, W. (1995). Proteasome from Thermoplasma acidophilum: a threonine protease. Science *268*, 579–582.

Seibert, M.M., Ekeberg, T., Maia, F.R., Svenda, M., Andreasson, J., Jönsson, O., Odić, D., Iwan, B., Rocker, A., Westphal, D., et al. (2011). Single mimivirus particles intercepted and imaged with an X-ray laser. Nature *470*, 78–81.

Shah, N.P., and Sawyers, C.L. (2003). Mechanisms of resistance to STI571 in Philadelphia chromosome-associated leukemias. Oncogene *22*, 7389–7395.

Shah, K., Liu, Y., Deirmengian, C., and Shokat, K.M. (1997). Engineering unnatural nucleotide specificity for Rous sarcoma virus tyrosine kinase to uniquely label its direct substrates. Proc. Natl. Acad. Sci. USA *94*, 3565–3570.

Shaw, D.E., Maragakis, P., Lindorff-Larsen, K., Piana, S., Dror, R.O., Eastwood, M.P., Bank, J.A., Jumper, J.M., Salmon, J.K., Shan, Y., and Wriggers, W. (2010). Atomic-level characterization of the structural dynamics of proteins. Science *330*, 341–346.

Sicheri, F., Moarefi, I., and Kuriyan, J. (1997). Crystal structure of the Src family tyrosine kinase Hck. Nature *385*, 602–609.

Sobolevsky, A.I., Rosconi, M.P., and Gouaux, E. (2009). X-ray structure, symmetry and mechanism of an AMPA-subtype glutamate receptor. Nature *462*, 745–756.

Solcan, N., Kwok, J., Fowler, P.W., Cameron, A.D., Drew, D., Iwata, S., and Newstead, S. (2012). Alternating access mechanism in the POT family of oligopeptide transporters. EMBO J. *31*, 3411–3421.

Sørensen, T.L., Møller, J.V., and Nissen, P. (2004). Phosphoryl transfer and calcium ion occlusion in the calcium pump. Science *304*, 1672–1675.

Srajer, V., Teng, T., Ursby, T., Pradervand, C., Ren, Z., Adachi, S., Schildkamp, W., Bourgeois, D., Wulff, M., and Moffat, K. (1996). Photolysis of the carbon monoxide complex of myoglobin: nanosecond time-resolved crystallography. Science *274*, 1726–1729.

Su, Y., Dostmann, W.R., Herberg, F.W., Durick, K., Xuong, N.H., Ten Eyck, L., Taylor, S.S., and Varughese, K.I. (1995). Regulatory subunit of protein kinase A: structure of deletion mutant with cAMP binding domains. Science *269*, 807–813.

Subramaniam, S., Hirai, T., and Henderson, R. (2002). From structure to mechanism: electron crystallographic studies of bacteriorhodopsin. Philos. Trans. A, Math. Phys. Eng. Sci. *360*, 859–874.

Sui, H., Han, B.G., Lee, J.K., Walian, P., and Jap, B.K. (2001). Structural basis of water-specific transport through the AQP1 water channel. Nature *414*, 872–878.

Sun, L., Zeng, X., Yan, C., Sun, X., Gong, X., Rao, Y., and Yan, N. (2012). Crystal structure of a bacterial homologue of glucose transporters GLUT1-4. Nature *490*, 361–366.

Sutherland, E.W., Jr., and Wosilait, W.D. (1955). Inactivation and activation of liver phosphorylase. Nature *175*, 169–170.

Tajkhorshid, E., Nollert, P., Jensen, M.O., Miercke, L.J., O'Connell, J., Stroud, R.M., and Schulten, K. (2002). Control of the selectivity of the aquaporin water channel family by global orientational tuning. Science *296*, 525–530.

Toyoshima, C., and Mizutani, T. (2004). Crystal structure of the calcium pump with a bound ATP analogue. Nature *430*, 529–535.

Toyoshima, C., and Nomura, H. (2002). Structural changes in the calcium pump accompanying the dissociation of calcium. Nature *418*, 605–611.

Toyoshima, C., Nakasako, M., Nomura, H., and Ogawa, H. (2000). Crystal structure of the calcium pump of sarcoplasmic reticulum at 2.6 A resolution. Nature *405*, 647–655.

Toyoshima, C., Nomura, H., and Tsuda, T. (2004). Lumenal gating mechanism revealed in calcium pump crystal structures with phosphate analogues. Nature *432*, 361–368.

Waight, A.B., Love, J., and Wang, D.N. (2010). Structure and mechanism of a pentameric formate channel. Nat. Struct. Mol. Biol. *17*, 31–37.

Waksman, G., Kominos, D., Robertson, S.C., Pant, N., Baltimore, D., Birge, R.B., Cowburn, D., Hanafusa, H., Mayer, B.J., Overduin, M., et al. (1992). Crystal structure of the phosphotyrosine recognition domain SH2 of v-src complexed with tyrosine-phosphorylated peptides. Nature *358*, 646–653.

Walter, M.R., Windsor, W.T., Nagabhushan, T.L., Lundell, D.J., Lunn, C.A., Zauodny, P.J., and Narula, S.K. (1995). Crystal structure of a complex between interferon-gamma and its soluble high-affinity receptor. Nature *376*, 230–235.

Wang, Y., Zhang, Y., and Ha, Y. (2006). Crystal structure of a rhomboid family intramembrane protease. Nature *444*, 179–180.

Wang, Y., Huang, Y., Wang, J., Cheng, C., Huang, W., Lu, P., Xu, Y.N., Wang, P., Yan, N., and Shi, Y. (2009). Structure of the formate transporter FocA reveals a pentameric aquaporin-like channel. Nature *462*, 467–472.

Wang, T., Fu, G., Pan, X., Wu, J., Gong, X., Wang, J., and Shi, Y. (2013). Structure of a bacterial energy-coupling factor transporter. Nature *497*, 272–276.

Ward, A., Reyes, C.L., Yu, J., Roth, C.B., and Chang, G. (2007). Flexibility in the ABC transporter MsbA: Alternating access with a twist. Proc. Natl. Acad. Sci. USA *104*, 19005–19010.

Wasmuth, E.V., Januszyk, K., and Lima, C.D. (2014). Structure of an Rrp6-RNA exosome complex bound to poly(A) RNA. Nature *511*, 435–439.

Watson, J.D., and Crick, F.H. (1953). Molecular structure of nucleic acids; a structure for deoxyribose nucleic acid. Nature *171*, 737–738.

Weyand, S., Shimamura, T., Yajima, S., Suzuki, S., Mirza, O., Krusong, K., Carpenter, E.P., Rutherford, N.G., Hadden, J.M., O'Reilly, J., et al. (2008). Structure and molecular mechanism of a nucleobase-cation-symport-1 family transporter. Science *322*, 709–713.

Widdas, W.F. (1952). Inability of diffusion to account for placental glucose transfer in the sheep and consideration of the kinetics of a possible carrier transfer. J. Physiol. *118*, 23–39.

Wiesmann, C., Fuh, G., Christinger, H.W., Eigenbrot, C., Wells, J.A., and de Vos, A.M. (1997). Crystal structure at 1.7 A resolution of VEGF in complex with domain 2 of the Flt-1 receptor. Cell *91*, 695–704.

Wing, R., Drew, H., Takano, T., Broka, C., Tanaka, S., Itakura, K., and Dickerson, R.E. (1980). Crystal structure analysis of a complete turn of B-DNA. Nature *287*, 755–758.

Wolberger, C., Dong, Y.C., Ptashne, M., and Harrison, S.C. (1988). Structure of a phage 434 Cro/DNA complex. Nature *335*, 789–795.

Wright, C.S., Alden, R.A., and Kraut, J. (1969). Structure of subtilisin BPN' at 2.5 angström resolution. Nature *221*, 235–242.

Wu, Z., Yan, N., Feng, L., Oberstein, A., Yan, H., Baker, R.P., Gu, L., Jeffrey, P.D., Urban, S., and Shi, Y. (2006). Structural analysis of a rhomboid family intramembrane protease reveals a gating mechanism for substrate entry. Nat. Struct. Mol. Biol. *13*, 1084–1091.

Wu, J., Brown, S.H., von Daake, S., and Taylor, S.S. (2007). PKA type IIalpha holoenzyme reveals a combinatorial strategy for isoform diversity. Science *318*, 274–279.

Wyckoff, H.W., Hardman, K.D., Allewell, N.M., Inagami, T., Johnson, L.N., and Richards, F.M. (1967). The structure of ribonuclease-S at 3.5 A resolution. J. Biol. Chem. *242*, 3984–3988.

Xie, T., Yan, C., Zhou, R., Zhao, Y., Sun, L., Yang, G., Lu, P., Ma, D., and Shi, Y. (2014). Crystal structure of the γ-secretase component nicastrin. Proc. Natl. Acad. Sci. USA *111*, 13349–13354.

Xu, W., Harrison, S.C., and Eck, M.J. (1997a). Three-dimensional structure of the tyrosine kinase c-Src. Nature *385*, 595–602.

Xu, Z., Horwich, A.L., and Sigler, P.B. (1997b). The crystal structure of the asymmetric GroEL-GroES-(ADP)7 chaperonin complex. Nature *388*, 741–750.

Xu, K., Zhang, M., Zhao, Q., Yu, F., Guo, H., Wang, C., He, F., Ding, J., and Zhang, P. (2013). Crystal structure of a folate energy-coupling factor transporter from Lactobacillus brevis. Nature *497*, 268–271.

Yamashita, A., Singh, S.K., Kawate, T., Jin, Y., and Gouaux, E. (2005). Crystal structure of a bacterial homologue of Na+/Cl−dependent neurotransmitter transporters. Nature *437*, 215–223.

Yang, W., Hendrickson, W.A., Crouch, R.J., and Satow, Y. (1990). Structure of ribonuclease H phased at 2 A resolution by MAD analysis of the selenomethionyl protein. Science *249*, 1398–1405.

Yin, Y., He, X., Szewczyk, P., Nguyen, T., and Chang, G. (2006). Structure of the multidrug transporter EmrD from Escherichia coli. Science *312*, 741–744.

Young, M.A., Gonfloni, S., Superti-Furga, G., Roux, B., and Kuriyan, J. (2001). Dynamic coupling between the SH2 and SH3 domains of c-Src and Hck underlies their inactivation by C-terminal tyrosine phosphorylation. Cell *105*, 115–126.

Zhang, X., Gureasko, J., Shen, K., Cole, P.A., and Kuriyan, J. (2006). An allosteric mechanism for activation of the kinase domain of epidermal growth factor receptor. Cell *125*, 1137–1149.

Zhang, X., Jin, L., Fang, Q., Hui, W.H., and Zhou, Z.H. (2010). 3.3 A cryo-EM structure of a nonenveloped virus reveals a priming mechanism for cell entry. Cell *141*, 472–482.

Zhang, P., Smith-Nguyen, E.V., Keshwani, M.M., Deal, M.S., Kornev, A.P., and Taylor, S.S. (2012). Structure and allostery of the PKA RIIβ tetrameric holoenzyme. Science *335*, 712–716.

Zhou, Y., Morais-Cabral, J.H., Kaufman, A., and MacKinnon, R. (2001). Chemistry of ion coordination and hydration revealed by a K+ channel-Fab complex at 2.0 A resolution. Nature *414*, 43–48.

Zhou, L., Hang, J., Zhou, Y., Wan, R., Lu, G., Yin, P., Yan, C., and Shi, Y. (2014). Crystal structures of the Lsm complex bound to the 3′ end sequence of U6 small nuclear RNA. Nature *506*, 116–120.